Surface Oxides on Advanced High Strength Steels (AHSS): Effect on Applications and Appearance.

By

Edward Tinashe Simbanegavi

[redacted]

(MSc by Research) Materials Engineering

Swansea University (2021)

Declarations

This work has not previously been accepted in substance for any degree and is not being concurrently submitted in candidature for any degree.

Signed: Simbanegavi, Edward Digitally signed by Simbanegavi, Edward
Date: 2022.10.10 18:29:36 +01'00'

Date: 10/10/2022

This thesis is the result of my own investigations, except where otherwise stated. Other sources are acknowledged by footnotes giving explicit references. A bibliography is appended.

Signed: Simbanegavi, Edward Digitally signed by Simbanegavi, Edward
Date: 2022.10.10 18:29:26 +01'00'

Date: 10/10/2022

I hereby give consent for my thesis, if accepted, to be available for photocopying and for inter-library loan, and for the title and summary to be made available to outside organisations.

Signed: Simbanegavi, Edward Digitally signed by Simbanegavi, Edward
Date: 2022.10.10 18:29:46 +01'00'

Date: 10/10/2022

The University's ethical procedures have been followed and, where appropriate, that ethical approval has been granted.

Signed: Simbanegavi, Edward Digitally signed by Simbanegavi, Edward
Date: 2022.10.10 18:30:07 +01'00'

Date: 10/10/2022

Abstract

1.1. The Thesis Structure

The structure of the thesis is as follows:

- Chapter 1: is an introductory chapter providing an overall summary of the work carried out during this project.
- Chapter 2: is a literature review; this aims to establish what is already known about the issue, what previous work has focused on and an investigation into performance in relation to certain applications.
- Chapter 3: will provide a background on the different characterisation techniques to be used i.e., how the analysis works and a justification as to why those techniques were chosen.
- Chapter 4: is a discussion and evaluation of the results obtained from the analysis; majority of these results will be related to existing literature to predict the outcome they would have within certain applications.
- Chapter 5: contains the overall research conclusions.
- Chapter 6: includes the proposals and work moving forward.

During the annealing of advanced high strength steels (AHSS) in a continuous annealing and processing line (CAPL), alloying elements with a high Oxygen affinity diffuse to the surface causing external oxidation. This results in a surface discolouration that is a departure from the typical finish observed in dual phase (DP) AHSS steels, which are a type of first generation (1G) AHSS. This can result in decreased confidence in the product's performance from the customer's perspective. Therefore, it is important to characterise the surface, and investigate any potential impact on performance. Previous work carried out with regards to applications i.e., contact resistance, highlighted that the darker samples exhibited higher contact resistance values, which would in turn negatively impact their welding performance. Therefore, it is important that surface chemistry be analysed i.e., oxides' phases be identified; the elements responsible to establish their effect on e.g., wetting performance. It is also important that this work needs to be accessible to both technical and non-technical users. The following research focused on analysis of both 'best and worst case' scenarios with regards to surface discolouration for DP800 and DP1000 grade AHSS. The characterisation of the oxide layer has been carried out using optical microscopy, scanning electron microscopy (SEM), energy dispersive spectroscopy (EDS) and x-ray photoelectron spectroscopy (XPS). SEM and EDS results showed that whilst there were alloying elements present within the oxide layer for both grades of metal, the cross-sectional width of this layer was very small. XPS was also carried out to complement/verify the EDS results. XPS analysis showed that alloying elements such as Mn and Cr diffused to the surface to form oxides (Mn2p, Cr2p) these oxides and Carbonates (Ca2p) are responsible for the surface discolouration observed. This was shown by the concentration of O1s with the typical binding energy for the metal oxides coupled by the peaks for the following spectra: $Mn2p_{1/2}$ and $Mn2p_{3/2}$ and $Cr2p_{3/2}$. The quantity was measured as % atomic concentration of the peak fitted models, this was shown to vary for all the samples depending on the severity of the discolouration i.e., the more discoloured the samples, a higher

% atomic concentration was observed at the surface. TalySurf surface roughness average values showed that for the DP1000 (C9321101), DP800 (C7025701) and (6491201) showed very little deviation for majority of the values despite the difference in surface appearance. This is likely due to all samples had to be within the release criteria for roughness for optimal performance in applications such as coating, therefore it can be concluded that surface appearance has a negligible effect on average roughness (Ra), maximum height above (Rp) and below (Rv) the mean line, Rsk was negative for all samples showing the presence of holes on the surface. DP800 had high root mean squared roughness values (Rsk) showing a high number of peaks and valley for the sample. Rv>Rp meant all samples regardless of grade has deeper valleys compared to peaks.

Acknowledgements

In no order, I would like to thank Tata Steel and the Materials and Manufacturing Academy (M2A) team in conjunction with Swansea University for their continuous support throughout the duration of my research. I would also like to thank my supervisors, Dr Zak Abdallah, Dr Christopher Mills, and Dr Ashley Willow for their support they have shown throughout the course of my studies. With their frequent feedback, meetings, and advice, I am grateful for it has helped elevate the overall quality of my thesis.

I would also like to thank Pete Davies and James Russell for allowing me access to the AIM facilities, Tom Dunlop for the XPS assistance, Dr H Lee and James Grant for the initial Raman training and access to the spectrometer. Lastly, I would like to thank my family, the friends I have met along the way, especially Darren Kappala-Ramsamy for the support that has enabled me to achieve this piece of work.

Table of Contents

List of Tables

List of Figures

Abbreviations

AHSS – Advanced High Strength Steel

All elements are described as their symbols, compounds are defined before abbreviation.

ATR – Attenuated Total Reflectance

BCC – body centred cubic.

BCT – body centred tetragonal.

CAPL – Continuous Annealing and Processing Line

CR - Cold Rolled

DP – Dual Phase

SEI – Secondary Electron Image

EDS – Energy-dispersive X-ray Spectroscopy

FTIR – Fourier Transform Infrared Spectroscopy

GDOES – Glow-discharge emission spectroscopy

HSLA – High Strength Low Alloy

NOK – samples deemed non satisfactory by the customer.

OK – samples deemed satisfactory by the customer.

SEM – Scanning Electron Microscopy

ULC – Ultra Low Carbon Steel

UHSS – Ultra High Strength Steel

XPS - X-ray Photoelectron Spectroscopy

Chapter One

1. Introduction

1.1. Background and Overview

As part of the ongoing pursuit to reduce emissions, the demand for Advanced High Strength Steels (AHSS) have increased, these have sheets of a thinner gauge, therefore offer reduced fuel use in vehicles due to their reduced weight [1]. The processing of these steel grades usually results in the formation of surface oxides because of the combination of the annealing environment and the Oxygen affinity of certain alloying elements [2]. This external oxidation is responsible for the surface discolouration observed on the processed steel; therefore, it is characterised, whilst also investigating its impact on applications such as welding, and coating. Characterisation can also allow the development of a dependable colour chart to function as a guide i.e., determining the suitable application for the steel based off the extent of oxidation as determined by the level of surface discolouration. Surface oxides in dual phase (DP) AHSS are inevitable, due to the combination of high temperatures in a wet annealing atmosphere and the Oxygen affinity of the alloying elements. This is due to intercritical annealing in the ferrite-austenite two phase temperature range, followed by rapid cooling transforming the intercritical austenite into martensite. These oxides are significantly more stable than the iron (Fe) oxides, therefore they cannot be reduced in these annealing atmospheres [3].

Whilst most surfaces eventually passivate, it is important to establish the extent of this oxidation and the implications this will have on the performance of the product. This is of relevance to the manufacturer as most clients are likely to return products, they would deem not ok (NOK) based of visual inspection, they would be less confident of the material's ability to meet the performance requirements e.g., weldability and their ability to be coated. Establishing the extent of any implications of these surface oxides is a potential money saver, as both manufacturer and customer will have the scientific evidence required to confidently conclude whether the effect is significant enough to warrant an action. Previous work that has been carried out on surface oxides in Steel, AHSS focused primarily on their impact on weldability. The conclusion determined that despite the difference in contact resistance between the discoloured samples, this was very minimal and fell within the existing acceptable range for welding therefore, the effects were negligible. However, for samples that were dark grey, dull surface appearance they showed a higher contact resistance value 2.5 times greater than the accepted maximum values for welding[4].

1.2. Aims and Objectives.

The following aims are to be completed by the end of the project.

- To propose a quick method of characterising the surface of AHSSs i.e., cross-sectional width and the roughness values for the OK and NOK samples.
- To evaluate different quantitative characterisation methods, summarising their effectiveness, assessing whether to recommend them for future use.

1.3. Justification of the project

Dual Phase (DP) used for this research is mainly used for Body in white (BIW), therefore it must exhibit welding reactive property values. Surface oxidation is a direct result of the annealing atmosphere, it can also be aided further compromises within the CAPL's fan seals. This would introduce more oxidation which at high temperatures forms oxide phases with the high Oxygen affinity alloying elements.

With an ever-growing emphasis on the improvement in sustainability in the automotive sector, AHSS have seen an increase in demand. This is due to the increasingly stringent legislation dictating the minimisation of the impact of car emissions on the environment. Therefore, for the Tata steel it is important that the production be further streamlined to maximise the capacity to cater to the growing demand. According to the Allied Market Research, in 2018, the AHSS market generated $12.80 billion, and this is estimated to grow to $33.85 billion by 2026, rising at a compound annual growth rate of 13.1% from 2019 to 2026 [5]. Previous work on surface oxides in AHSS has focused on the impact surface oxidation had on galvanising. It proved that despite the segregation of Mn to form Mn oxides on the surface, the samples still exhibited good coating adherence and a well-developed inhibition layer [6]. Conventional characterisation methods employed are highly technical, therefore cannot be easily adopted into the production line, neither can they be easily interpreted by a non-technical user. For this reason, this project aims to further simplify the process of surface oxidation recognition and move it forward to practical applications.

1.4. Methodology

The research will involve the analysis of the C7025701-DP800 and the C9321101-DP1000 coil samples alongside edge samples from the 6491201-DP800 coil which showed the most severe discolouration. To fulfil this, characterisation techniques ranging from optical microscopy to quantitative techniques such as XPS will be employed. The use of quantitative techniques allows the evaluation of whether a relationship can be established between surface appearance and the elemental composition of each coil. SEM will allow greater magnifications to measure the widths of the oxide layers within each sample, BSE and EDS are also carried out i.e., to identify the chemical composition of the oxide layer and the substrate. This is useful to establish if the oxidation is indeed concentrated on the surface (majority of it occurring externally). XPS allows a detailed observation of the physical and chemical interactions occurring at the surface, including establishing the chemical composition and the oxide phases. This is important as it allows easy identification of the oxides that may be on the surface and a

differentiation if one exists between the samples analysed. SEM will also allow the extent of the oxidation to be evaluated and this can also be used to build a picture of whether a relationship can be confidently established between appearance and the extent of external oxidation.

Performance in applications can be assessed using literature reviews, this allows the final proposal to be justified against the overall impact i.e., if purely aesthetic (there is no notable impact on performance), instead of proposing a quick characterisation technique to pinpoint samples whose performance maybe hindered, an explanation can be issued to be interpreted by both technical and non-technical customers highlighting the extent. EDS and SEM are performed simultaneously using the different detectors mounted in the same microscope. This is carried out to perform preliminary identification of the elements present on the cross-sectional surface by carrying out both spot and area scans to produce spectra for the oxide layer and the substrate.

Project plans

Due to the covid pandemic, there were disruptions with regards to accessing certain labs and therefore, some of the analysis could not be completed within the original period as highlighted in Table 1. In the end the project was completed, with outcomes proving to be representative of the situation i.e., what was already known by the manufacturer.

Table 1: The initial project plan and the amendments made during the extension period.

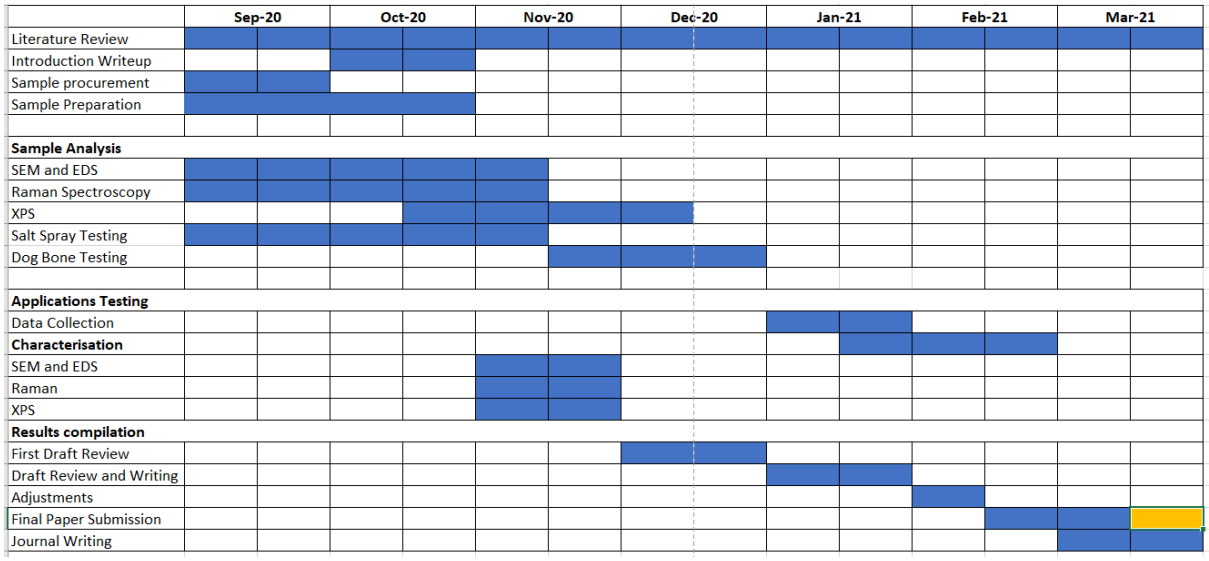

Chapter Two

2. Literature Review

2.1.The role of alloying elements in steels

To gain an appreciation of the problem, it is important that one understands the formation of these steel grades, the justification for the inclusion of certain alloying elements, the annealing environment. In general, Carbon (C) is the most essential alloying element, the strength, hardness, hardenability positively correlates with the Carbon content up to ≈0.6wt%. On the contrary, toughness and ductility decrease as Carbon content increases. The Silicon (Si) deoxidises and increase ferrite strength without a serious loss to ductility. The Manganese (Mn) is used in most steels as it deoxidises the melt, facilitating hot working of steel by reducing the impact of Sulphur (S) content. The Chromium (Cr) increases corrosion resistance and oxidation, high temperatures strength, hardenability, and abrasion resistance in high Carbon alloys. The Aluminium (Al) is responsible for controlling the grain size and deoxidising the steel. The Boron (B) significantly increases hardenability, especially for low Carbon alloys, while the Calcium (Ca) controls composition, type, shape, size, and distribution of oxide and/or sulphide inclusions improving ductility, impact strength and machinability. The Molybdenum (Mo) increases hardenability of steel, helping maintain a specified hardenability. The Nickel (Ni) in low alloy steels reduces sensitivity during heat treatment, this includes distortion and cracking when quenching. Ni also improves low temperature toughness and hardenability. The Niobium (Nb) lowers transition temperature and raises strength in low Carbon steel. Titanium (Ti) is added to Boron steels to combine with the Oxygen and nitrogen increasing the effectiveness of Boron [7][8].

2.2.DP AHSS Alloys

Dual Phase (DP) advanced high strength steels (AHSS) have enjoyed wide usage in the automotive industry due to their balance of strength, formability and ductility which comes from their composite microstructure, consisting of ferrite and martensite. The term DP refers to the fact that these steels consist of two phases, body centred cubic (BCC) ferrite α and body centred tetragonal (BCT) martensite ά, rich in Carbon [9]. The oxidation of steel due to heat treatment occurs principally due to the combination of the presence of Oxygen at high temperatures and the less noble alloying elements Mn, Al, Si and Cr. In a CAPL line this can be due to broken seals along the line letting Oxygen in, typically at the cooling fans. Therefore, it is important that an understanding of these oxides and establishing their impact i.e., the different elements' oxides and their respective phases, and the thickness of the layers and their subsequent impact on performance. Annealing of AHSS grades often results in surfaces covered by oxides due to alloying elements which diffuse to the steel surface during annealing and are oxidised by residual Oxygen from the furnace atmosphere [10]. For instance, Mn diffuses to the surface at ≈ 800°C and becomes oxidised [11].

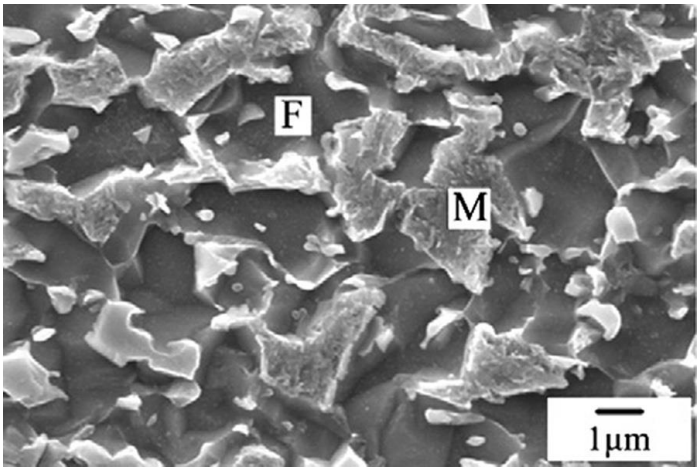

Figure 1: An SEM image of a DP AHSS microstructure showing ferrite (F) and martensite (M) [12].

Due to the growing need to improve efficiency in the automotive industry, AHSS will show an increase in both usage and demand due to their versatility and lighter weight. The better performance in crash energy management and superior strength allows performance to be achieved with thinner components, reducing vehicle weight as a result)[12]. An illustration of the use of DP in automotive application is shown in Figure 2.

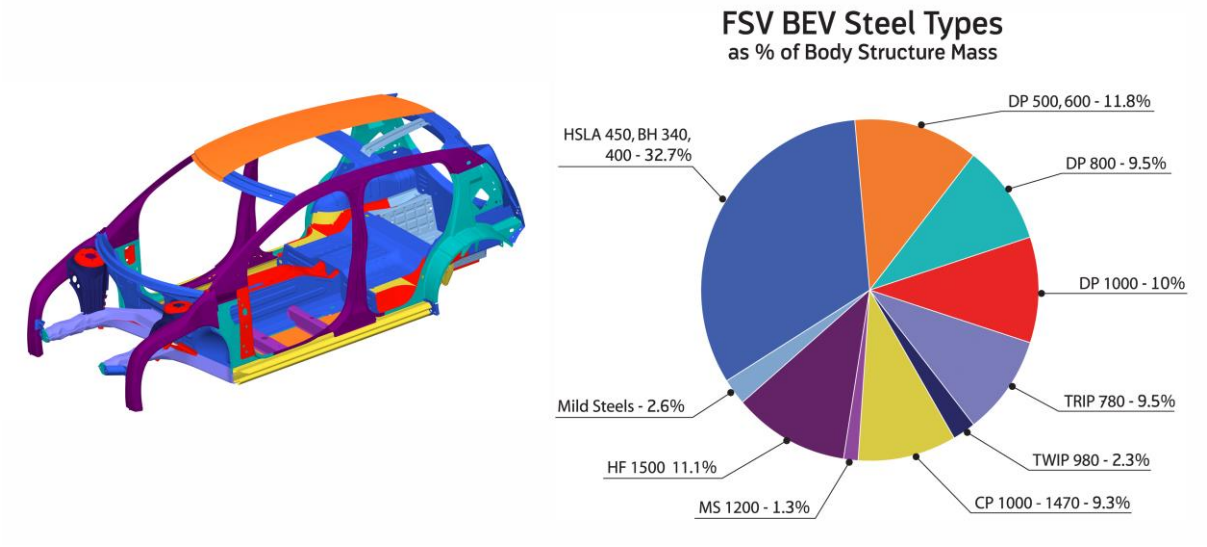

Figure 2: The use of different types of DP AHSS in an automotive body structure[1].

Applications of AHSS include use in body in white (BIW) within the automotive industry i.e., pillars, crash boxes and support components [13]. There are different types of DP AHSS grades whereby the mechanical properties do not yield a fixed figure due to the processing parameters and therefore, the mechanical properties exist within a defined range. The understanding of the primary uses of the AHSS manufactured by Tata Steel allows a focus on certain properties relevant to the consumer, i.e., their performance in applications. These properties are mainly heat transfer, friction, wear resistance, surface finish, welding, and coating of the material. The AHSS is suitable for these applications due to the ability to alter the mechanical properties by modifying the amount of Carbon, therefore, the optimum amount of martensitic component of the steel. As illustrated in Figure 3, the demand for AHSS from 2012 to 2025 in the US in

automotive applications is predicted to double in mass. UHSS in comparison will see steadier increase, it is still lower than that of AHSS.

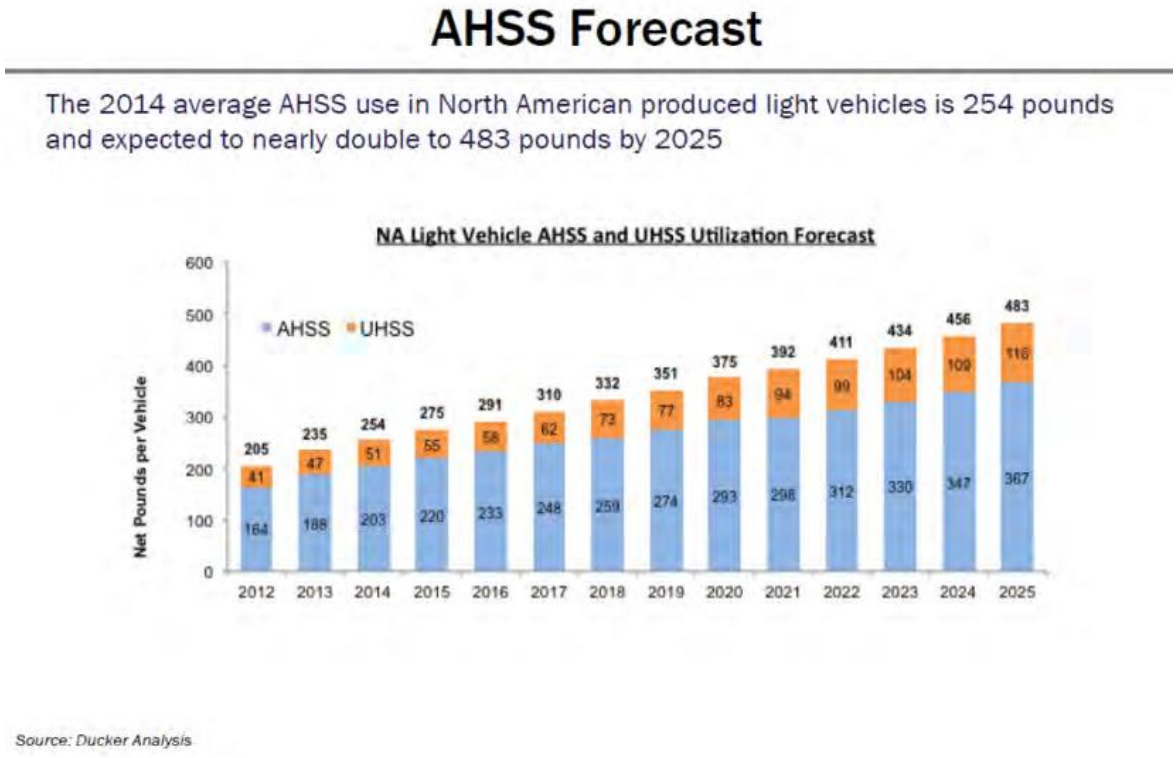

Figure 3: The forecast with regards to the utilisation of AHSS [14].

2.3.Colour development and effects on applications.

To understand the elements responsible for the multiple characteristics exhibited by DP AHSS such as their strength and ductility, an understanding of the different phases needs to be established. The shades observed on the surface of the steel are a direct result of light interference which correlates to the thickness of an oxide layer [15]. When light of a wavelength (λ) is reflected from metal covered with an oxide film, it is eliminated by destructive interference if the thickness of the oxide is 0.25 λ. This is due to the reflected beam having a path difference with the incident beam of 0.5 λ, thus leading to destructive interference. If the oxide layers increase in thickness, then they become opaque and interference through reflection from the metal surface is no longer feasible. Figure 4 shows the effect of destructive interference on surface appearance, and the wavelengths of different colours.

The colour on the surface of the DP samples can be attributed to various alloying elements within the AHSS DP grades and the extent to which oxidation has occurred. This can be further proven through multiple analysis methods such as X-ray photoelectron spectroscopy (XPS), these enable the quantification of elements within the oxide film. Some materials such as ultra-low Carbon (ULC) steel seem to not have as big an issue with surface discolouration. Therefore, it is also worth establishing the difference in composition to isolate any elements in

high wt% that could potentially be responsible for the discolouration. Non-metallic inclusions whilst positively impacting machinability can have an adverse impact on the mechanical properties and development of oxide layers due to the Oxygen affinity of the elements involved, consequently negatively impacting the corrosion resistance and weldability [16].

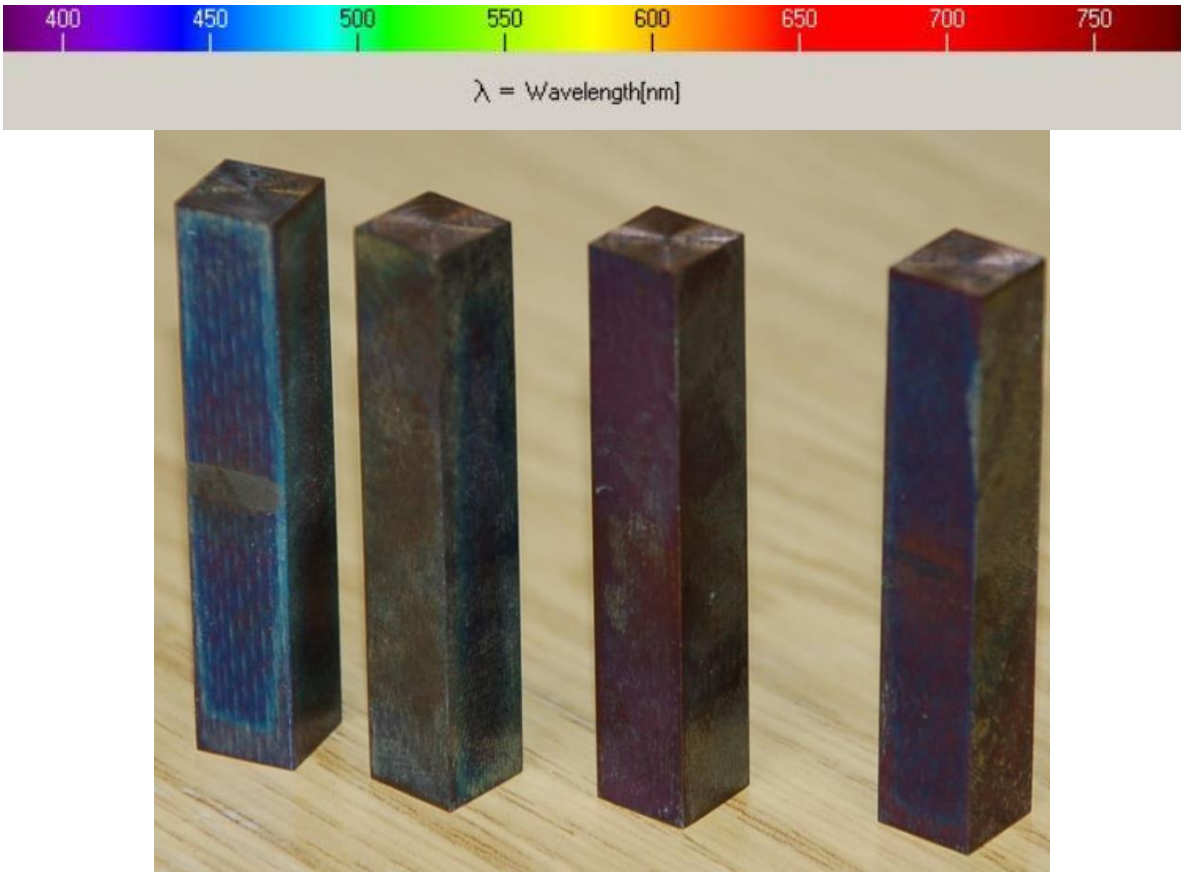

Figure 4: The effect on destructive interference on the surface appearance of different steel samples [16].

2.4. Possible solutions to effects on applications.

The friction between two solid surfaces in solid-state contact is the resistance to tangential motion of one surface over the other, whether that motion be sliding [17]. The influence of the presence of Oxygen on the welding and coating capabilities is a topic that has been explored previously in the field of tribology. Each material possesses a friction coefficient, and the effect of the oxide layers can be evaluated with each sample of steel exhibiting various forms of discolouration. The results would allow the determination of a coefficient of friction, and this can in turn be compared to that of an AHSS sample showing minimal discolouration (best case scenario). If the friction of the oxide sliding on the oxide is of a notable difference from that of the metal, then control measures must be proposed to minimise the effect of the oxide layer on the friction coefficient of the sample[17]. Method of study for these applications would involve measuring the electrical resistance between the sliding surfaces, if the resistance arises from a constriction in the current [18]. The voltage drop across the contacts is to be kept low enough such that heating, and breakdown effects can be minimised or eliminated if possible. The reduction of the oxide layer on the surface can be achieved using a variety of methods, there

are instances where oxide inclusion would have to be considered. The brittle oxide layers can be of two types: particles and films, the latter being a particular concern when it comes to potentially compromising the quality of the weld joint [19]. Once the impact of the oxide layer has been established and the elemental composition of the oxide layer has been confidently identified there might be needed to remove the oxide layer, and this can be achieved in a multitude of ways e.g., pickling. The pickling can be carried out with a single or mixed acid, and this can be carried out towards the end of the line before the sample is sent off to the customer. Previous work carried out with regards to selective oxidation has concluded that Oxygen affine elements such as Si, Mn, Cr are oxidised during annealing [20]. The knowledge of microstructure formation could prove useful going forward i.e., when the CAPL line is running. This helps evaluate the process routes, propose changes where appropriate, if the need to reduce the effect of oxide layers is justified. These can be further refined to be accessible to non-technical users to improve customer satisfaction. Due to the forecasted use of AHSS, it is important that characterisation methods and control measures be established early to ensure that customer satisfaction is guaranteed and there is sufficient evidence to establish whether surface shade impacts performance, if so, to what extent. Process control is critical with AHSS products, because the manufacturing window is significantly smaller compared to conventional steels [1].

2.5. The Problem Statement

Previous work carried out investigated the relationship between contact resistance and surface discolouration for the DP800 steel by Tata Steel R&D(A&E-J&P) on 1.85mm thick samples was further developed in this project. The dark coloured (NOK) sample (Coil ID C6416101) showed a higher contact resistance value of 0.275 mΩ with a standard deviation of 0.094mΩ. Compared to the OK sample values of 0.180mΩ and a standard deviation of 0.018mΩ. These values were taken across seven series of seven measurement points. On the other hand, previous work carried out on nine DP1000 samples from CAPL showed the contact resistance for samples with slight discolouration had small variations 0.428-0.622mΩ. Only the sample with a dark surface appearance showed a high contact resistance value of 2.5mΩ, this would have had a negative impact on performance. An illustratiion of the samples under investigation are shown in Figure 5, whilst Figure 6 highlights the values for contact resistance for all the samples under investigation. The conclusion of this study was that according to the ISO18594 standard for contact and resistance measurement, the darker samples had higher values for the spot weld and contact resistance tests, this was still within the welding range[4].

Figure 5: The two samples used in the contact resistance investigation [4]..

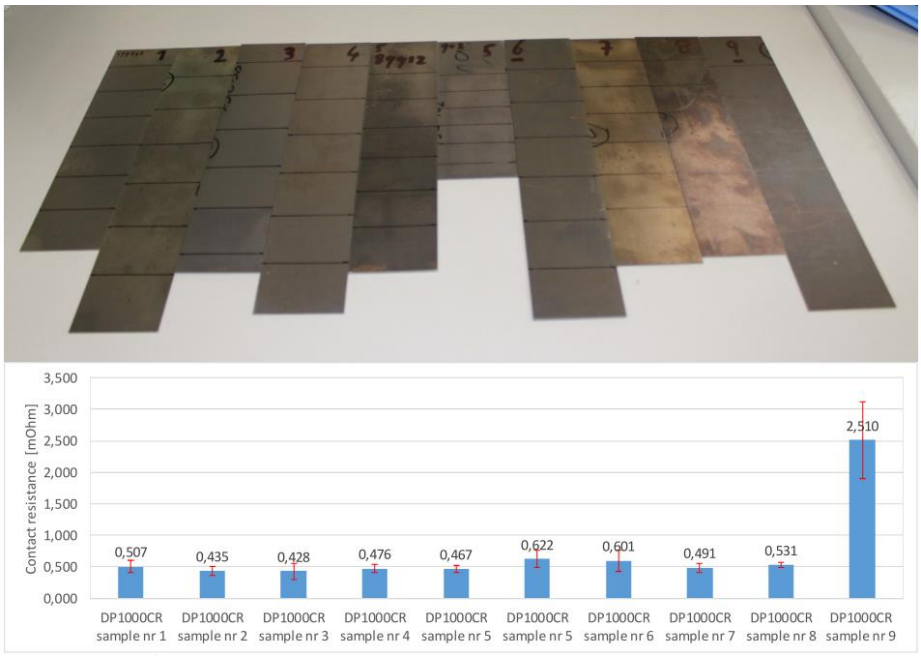

Figure 6: The DP1000CR samples used in the previous investigation and their contact resistance values [4]..

The main aim of this research is to establish a relationship between appearance and performance, and if necessary, propose a measure to minimise any negative effects from the oxide layer if present. Based on previous research both in house (Tata) and external, it is important to note that there is a potential impact on performance. An assessment still needs to be made in a manner that is adaptable into the production line to determine whether any control measures are warranted to reduce the oxide layer's impact e.g., whether picking is economically justifiable to eliminate this issue. Majority of the literature with regards to surface appearance has largely focused on the effects of the environment such as annealing atmosphere, dew points and the galvanising heat treatments. This research has been concerned with performance with regards to galvanising, it was established which elements were responsible

in Seyed Mousavi and McDermid's work on the Selective Oxidation of a C-2Mn-1.3Si (Wt Pct) Advanced High-Strength Steel During Continuous Galvanizing Heat Treatments[21]. Their work proved the effect of the combination of oxygen partial pressure, dew points and annealing time on the oxide layer. Si oxides were present externally at lower dew points (-50 degrees Celsius), whilst Mn was present at both lower and higher (+5 degrees Celsius), but Si oxides were internally, longer annealing times increased internal oxidation.

It is also worth noting that these investigations were in controlled environments aimed at establishing process control. The research to be carried out in this paper is directed at the finished product, establishing the link between colour and performance in other applications such as welding having built from previous work carried out by Tata. Most of the analysis equipment used in the literature is not adaptable into a CAPL line i.e., Transmission Electron Microscopy (TEM) is highly technical therefore any results produced from the research cannot be easily interpreted by a potential customer or any non-technical user. Their work also established the correlation between longer annealing times and the thickness of the oxide layer and the internal oxidation that occurred with the Mn[22]. Most importantly it was discovered that the presence of Manganese (Mn) oxides at the steel surface did not hinder the samples from exhibiting good coating performance [6]. This was attributed to the aluminothermic reduction of the Mn oxides by the Al present in the Zn bath followed by the reactive wetting between the substrate and the Zn bath. G. Seyed Mousavi and J. R. McDermid also focused on the effect of increasing annealing atmosphere oxidising potential's effect on reducing external surface selective oxidation on DP. R. Khondker, A. Mertens, and J. R. Mcdermid's research has established that the annealing atmosphere influences the surface condition as alloying elements segregate i.e., giving rise to selective Mn oxidation which was more external than internal when the oxidation potential of the atmosphere increased from pH_2O/pH_2 of 0.00844 to 0.03451 [6]. There was also an observation made with regards to the transition from external to internal oxidation occurring when the oxidation potential of the atmosphere increased. The research into the DP800 and DP1000 can fill a gap in the knowledge with regards to the exacting conditions of the CAPL line and the surface appearance of the products, the subsequent quantification using XPS can then establish the impact of oxidation phases, dew points, cooling rates and the annealing atmosphere Oxygen potential (pH_2O/pH_2 ratio).

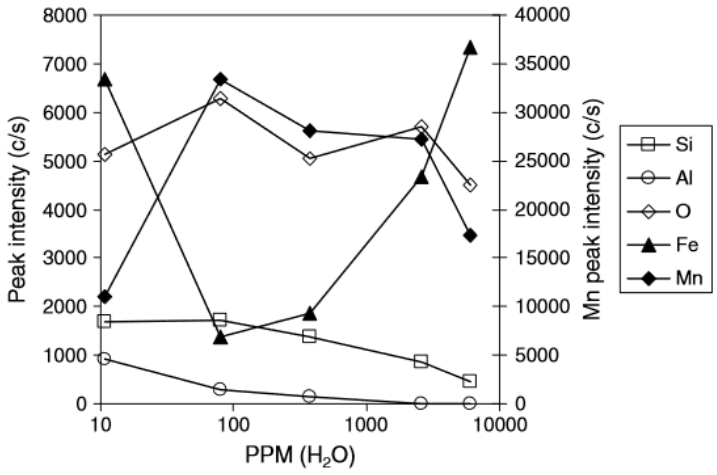

Figure 7: XPS results for the Mn peak intensity for a sample relative to the wet atmospheres.

Chapter Three

3. Characterisation

Analysis techniques together with data interpretation software allow for easy identification of the elements responsible for surface appearance in the DP AHSS samples. In addition, developments regarding the adoption of a colour gradient chart (ImageJ), can be used to conclude whether a certain batch is suitable for the applications desired by the customer. The Energy Dispersive Spectroscopy EDS can be adopted to map out the distribution of certain elements within the cross section of the sample. The use of X-ray Photoelectron Spectroscopy (XPS) facilitates the analysis of the oxidation states of the alloying elements whilst making a comparison between the external and internal oxidation. The analysis techniques used are primarily to quantify the oxide layers present to draw the comparisons between the different surface appearances for both similar and dissimilar grades. The latter allows for a comparison to be made with regards to the different wt% of alloying elements and the associated effects on the oxide layer, and the phases they would exist in. The roughness measurements were carried out to determine the implication the surface appearance would potentially have on the coating performance of the samples. Optical microscopy, Scanning Electron Microscopy (SEM), Energy Dispersive Spectroscopy (EDS) X-ray Photoelectron Spectroscopy (XPS), TalySurf roughness measurement are to be used during this research. Some analysis methods listed previously were evaluated with regards to their relevancy to the research project and the return of investment i.e., how much time would be devoted to them as a percentage of the duration of the whole project. The following paragraphs will offer a more in-depth explanation of the analysis techniques and an evaluation of their relevance to the research carried out. Samples were prepared and plasma cleaned before SEM and EDS are carried out.

3.1. X-ray photoelectron spectroscopy (XPS)

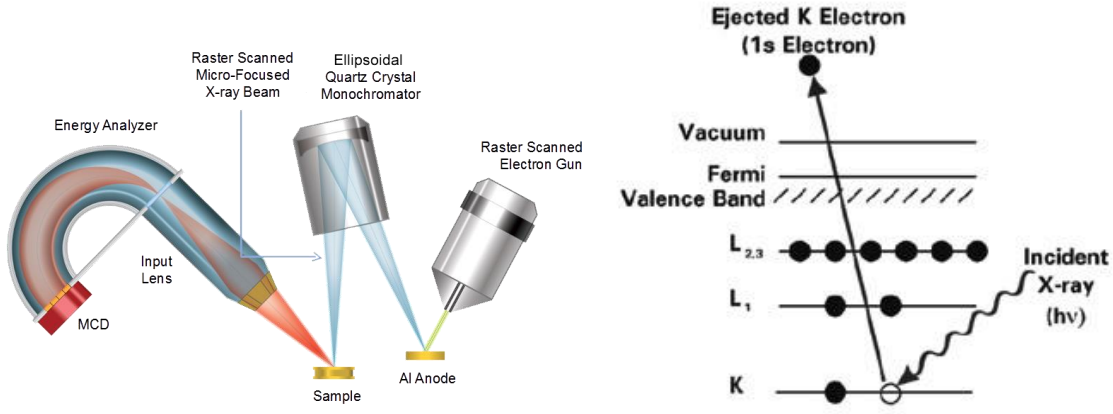

Figure 8: A typical setup when analysing a sample using XPS[23].

The XPS method, Figure 8 is a quantitative technique that involves the excitement of the atom's core electrons then subsequently measuring the kinetic energy of the excited electrons. The discs represent electrons, and the bars represent electrons; bars represent energy levels within the material undergoing analysis. The equation governing the process is KE = hv – BE [22].

The use of XPS would allow the identification of elements within the oxide layer and their phases, to identify the oxide. The wt% of the oxide can be referenced for future analysis on performance, to establish their effect on contact resistance, coating, surface finish and friction. The peaks correspond with the binding energy of the core electrons and their unique position allows identification of the atoms. XPS is a suitable analysis method across a wide range of applications previously outlined (friction, surface properties and adhesion). This analysis method is used extensively to characterise both surface and internal chemistry of conductive samples, it can measure the elemental composition, empirical formula, chemical state, and electronic state of the elements within a material [23].

When carrying out depth profiling, analytes detected from the surface i.e., from the oxide would be stronger than those detected deeper into the sample and therefore there is an exponential attenuation function as depth increases. This is minimal if the oxide layers observed will be less than10nm (ultrathin films), it is still worth acknowledging the reduced number of emitted photoelectrons as depth increases due to e.g., inelastic collisions and entrapment etc. To reduce the effect of surface contamination it is important that the samples are cleaned, using a hexane solvent that minimises damage to the oxide layer [24] or alters its state compared to as received. It is also important that other techniques be used to complement the findings from XPS such as FTIR as discussion cannot be advanced based on the findings of this singular technique [25]. Previous work has been carried out using XPS to investigate the effect of dew point on selective oxidation in dual phase steels. This method of analysis used the peak kinetic energy to determine the surface coverage the presence of an oxide layer using the unique kinetic energy (binding energy) of the individual compounds (oxides) within the surface. Previous surface characterisation using XPS has shown very high levels of reproducibility if sample preparation is standard i.e., the binding energy was found to be within ±0.3eV [26]. There is an underlying assumption that is required to quantify an XPS spectra, this assumption is that the number of electrons recorded is proportional to the number of atoms in each state[27]. When comparing samples, peak areas are not a recommended means as not all electrons leaving the sample surface are detected. The reliable way of comparing two samples is the use of percentage atomic concentration (% atomic concentration). The selection of which transition to use for quantification is decided using the transition with the largest peak area, free from interfering peaks. Lastly, it is also important to note that for some binding energies, there is a shift relative to their state during analysis. To ensure the results are reliable it is important to keep the standard deviation below 1, this can be difficult for elements with overlap.

3.2. Scanning Electron Microscopy (SEM)

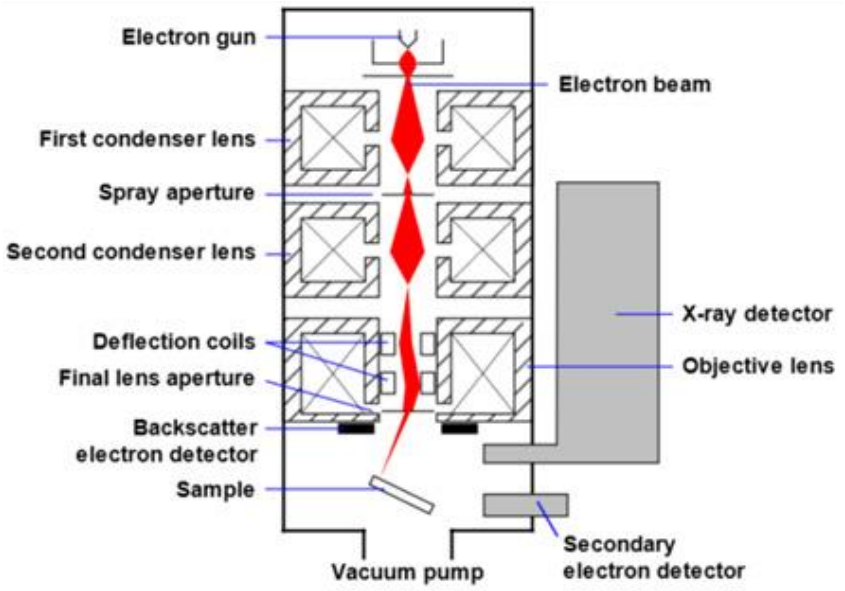

Figure 9: Shows a schematic of a typical SEM setup [28].

As Figure 9 illustrates, in SEM, the electron gun generates a beam of energetic electrons down a column onto a series of electromagnetic lenses which focus the incident electron beam that scans the sample in a raster pattern (spot scanning can also be used, mainly during EDS) [29]. This beam can be adjusted to alter the scanned area and the magnification (µm). When the incident electrons interact with the surface of the sample, the energetic electrons released from the sample surface producing different scatter patterns which are then used to determine certain properties such as size, shape, texture, and composition. There are numerous detectors available to capture the scattered electrons, including secondary and backscattered electrons and X-rays [30]. Backscatter electrons are incidental electrons reflected backwards; and the images produced by these electrons are used to obtain the elemental and compound compositional data (x-rays produced can also be used to gather similar data). Diffraction of the backscatter electrons can be attributed to the crystalline structure of the AHSS, and this will allow us to determine the orientation of the sample. Figure 9 illustrates the working principle of the SEM.

SEM has been employed using the Advanced Imaging of Materials' Zeiss EVO LS25 device, to gain insight into the materials topography and composition [30]. This analysis technique has its limitations with regards to conductivity i.e., when carried out using nonconductive polyester resin which might be used to protect the structural integrity of sensitive oxides. This would require the use of conductive tape (in this case Aluminium tape) or Carbon coating of the sample, image quality could still not be as sharp as a conductive sample. The SEM is a very useful analysis technique to establish the oxide layer's thickness as it allows direct measurement of the width of the oxide layer at a high magnification (µm), isolating the worst-case scenarios i.e., thickest oxide layer or calculating an average in terms of thickness. Given the time taken to setup the machine and its availability it is advisable that multiple samples be mounted simultaneously to complete workloads quicker. The location of the SEM equipment

must be independent of vibration, ambient magnetic and electric fields to ensure optimum results are achieved.

3.3. The Energy Dispersive Spectroscopy (EDS)

Another analysis method: EDS, will allowed a detailed look at the metal-oxide boundary and enabling a distinction in terms of composition of the AHSS when to the oxide layer. This method of analysis provides both a qualitative and quantitative view of the sample with regards to its microstructure and the composition. An EDS detector was incorporated into the SEM machine and uses the X-ray detector in conjunction with separate interpretation software to collect and analyse the energy spectra. This form of analysis is especially useful for observation of multiple samples given how quickly data can be gathered and given proximity to the sample. The working distance allows gathering of a greater number of X-rays and therefore improving the accuracy and reliability of the sample due to the higher detector efficiency. The EDS covers most of the elements with an atomic number greater than that of Carbon (C), lighter elements can be difficult therefore if the sample were to be contaminated with lighter elements, detection would be problematic. EDS determines the energies of the X-Rays emitted from the area being excited by the electron beam, this mode of operation is more qualitative than is quantitative [31]. This analysis technique involves the use of X-rays on the sample's cross section for a particular area, this can be carried out in predetermined spots or map an area i.e., show distribution of the elements on the cross section. Furthermore, this technique is non-destructive, therefore can be considered for characterising products to be sent to customers. Data was collected and interpreted using Oxford Instruments software.

3.4. Optical Microscopy

Analysis carried out using an optical microscope (Zeiss Primotech) on the surface allowed a more distinct and detailed look at the difference in the colours at the surface and the surface structure due to the shapes observed on the surface. Extended depth of field was used to focus different parts of the sample to ensure the final image was completely focused. This form of microscopy is also employed during sample prep to analyse whether there are still scratches on the surface when polishing the samples. Due to the limitation in magnification, this technique was reserved mostly for the earlier stages of sample preparation, to reduce the potential of surface stains and scratches when preparing samples for the more sensitive methods of analysis. This allows for further distinction and an observation of the surface topography as illustrated in *Figure 11*.

3.5. TalySurf

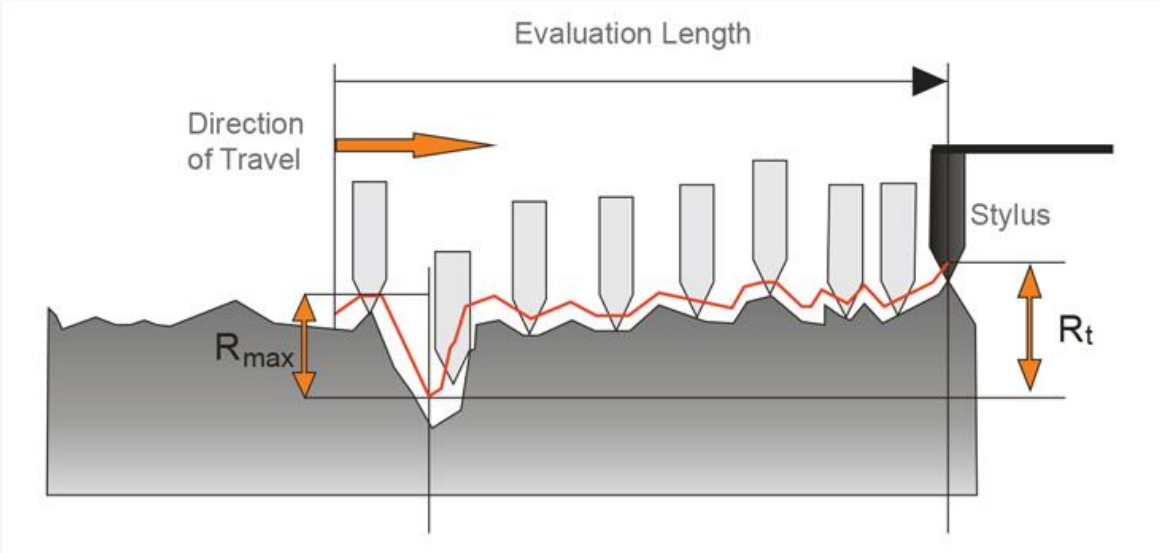

Figure 10: Shows the surface roughness values Rmax and Rt across an evaluation length in relation to the position of the stylus.

This method of measurement uses a stylus that is orientated perpendicular to the surface. The Ra value is the arithmetic average of surface heights measured across a surface[32]. The Ra is the average roughness profile and the mean line. The average maximum height of the profile is referred to as (Rz) this a useful measure as the Ra is quite insensitive to extremes, therefore if the distribution of the oxide layer on the sample is limited to certain samples this value is considered. The Rz samples five lengths and helps reduce the error and improve reliability of the data as it is less susceptible to scratches. The maximum height of the profile (Rt) is the distance between the highest and lowest points of the profile within the length under evaluation which can be affected by surface scratches, maximum peak height above the mean line is (Rp). The root mean square average of the roughness profile ordinates (Rq). Maximum profile valley depth (Rv) is the distance between the deepest valley and the mean line. The vertical distance from peak to valley (Rmax) is used to distinguish any anomalies such as scratches on the surface. The root mean square roughness (Rrms) is the same as (Rq). (Rsk) is a measure of symmetry (holes vs peaks) if this value is negative this shows that the surface is predominantly holes.

3.6. Sample Preparation

Samples were machined in the engineering workshop into 25mm squares, and the final samples chosen for analysis were picked through observing appearance under an optical microscope to determine the ‘best and worst’ scenarios from each original sample. Firstly, capture pictures of the surface, then mount the samples into Bakelite for SEM and EDS to be conducted, they are then ground and polished as detailed in the following paragraph.

Grinding and Polishing

Initially there were challenges involving automatic grinding as unfortunately the depth of the samples varied and therefore manual grinding was more suitable. All samples to be analysed using SEM and EDS were mounted in Bakelite, since the mount had to be conductive for analysis to take place. All four samples were ground in four steps with grades (120, 400, 600 and 1200nm) and subsequently polished using a water based lubricant diamond polish at a present rotation speed at 1, 3 and 6 microns.

During grinding a notch is made to orientate the samples, then a rotation of 45 degrees clockwise is made between each grade to reduce the possibility of a surface incline and reduce the effect of any prevalent scratches as you move up to finer grades. Samples are observed under a microscope between each polishing grade to ensure there are uniform finishes on the surface before progressing to the next stage.

Chapter Four

4. Results

Six samples were collected in total, two from E1, E2 and the C7025701directional roll, these were graded based of their visual appearance and labelled A and B with the later signify a darker surface colour

The inclusion of the ultra-low Carbon (ULC) steel is for comparative reasons, as reported there was no surface discolouration with this grade, unless there was a major fault on the production line. The chemical composition allows for an initial comparison to be made with regards to which elements maybe responsible for the selective surface oxidation.

Table 2: Shows the typical/desired elemental composition for the grades analyses, DP800, DP1000 and Ultra low carbon provided by the supplier.

Element	DP800 (1/100) %	DP1000 (1/100) %	ULC (1/100) %
C	Aim:0.135 Min: 0.12 Max:0.15	Aim:0.15 Min:0.13 Max:0.162	Max:0.035
Si	Aim:0.25 Min:0.20 Max:0.30	Aim:0.05 Min:0.03 Max:0.07	Max:0.02
P		Min:0.009 Max:0.013	Max:0.017
Mn	Aim:1.82 Min:1.72 Max:1.92	Aim:2.20 Min:2.11 Max:2.29	Aim:0.1 Min:0.05 Max:0.25
Cr	Aim:0.55 Min:0.50 Max:0.60	Aim:0.55 Min:0.50 Max:0.60	Max:0.60
S.Al	Min:0.02 Max:0.08	Aim: 0.030 Min:0.015 Max:0.055	Aim:0.04 Min:0.02 Max:0.060
T.Al	Min:0.02 Max:0.085	Aim: 0.035 Min:0.020 Max:0.060	Aim:0.04 Min:0.02 Max:0.065
Nb	Aim:0.025 Min:0.02	Aim:0.015 Min:0.012	Max:0.010

Element	DP800 (1/100) %	DP1000 (1/100) %	ULC (1/100) %
	Max:0.03	Max:0.020	
Ti	Min:0.02 Max:0.04	Aim:0.022 Min:0.015 Max:0.029	Min:0.030 Max:0.085
Ca	Min:0.001 Max:0.070	Aim:0.0029 Min:0.0013 Max: 0.005	Max:0.0005
CEV	Aim:0.555 Min:0.530 Max:0.580	Min:0.01 Max: 9.99	Min:0.01 Max: 9.99

Table 2 highlights the typical elemental composition of the steels studied. For all the values obtained during analysis it is important to note that the distribution of the oxide across the surface of these AHSS is not uniform. These samples analysed were cut in a manner as to maximise the area where the oxide layer would be located therefore the SEM, EDS, XPS and TalySurf results are not representative of the sheet. Majority of these samples were located from the middle and edge of the sheets, a ‘best and worst’ case sample were chosen based on the level of discolouration they displayed on the surface through visual inspection.

4.1. Sample Matrix

Table 3 shows the cross-sectional width of all the samples that were analysed and the analysis techniques that were performed.

Table 3: Sample matrix of the samples that were used for the SEM, TalySurf and XPS analysis. Sample 1 and 2 denote samples chosen for a 'best' and 'worst' case scenario.

Sample ID (Coil ID)	DP1000 (C9321101)		DP800 Rolling Direction (C7025701)		E1 DP800 (6491201)		E2 DP800 (6491201)	
	A	B	A	B	A	B	A	B
Cross section width (mm)	0.88		0.74		1.99		1.99	
XPS	✓	✓	✓	✓	✓	✓	✓	✓
TalySurf	✓	✓	✓	✓	✓	✓	✓	✓
SEM	✓	✓	✓	✓	✓	✓	✓	✓

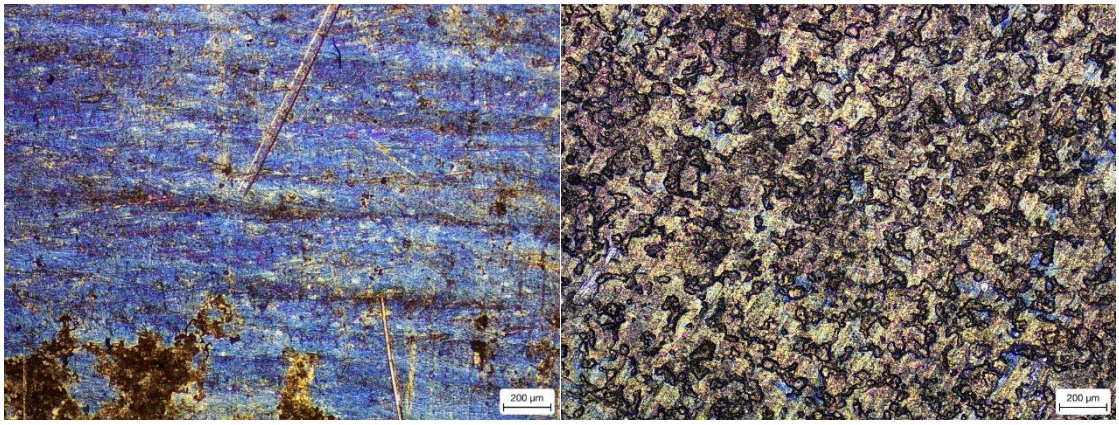

Figure 11: (L) The surface appearance of the C7025701(DP800) sample (left) and the C9321101(DP1000) sample (right) as observed under a 5x lens.

Figure 11 shows the difference in surface appearance at similar magnification for both the DP800 and DP1000 samples. DP800 shows a blue appearance on the surface, compared to DP1000 which presents a darker surface with tiny specs of blue present on the surface as well as pits.

4.2.C9321101 (DP1000)

SEM

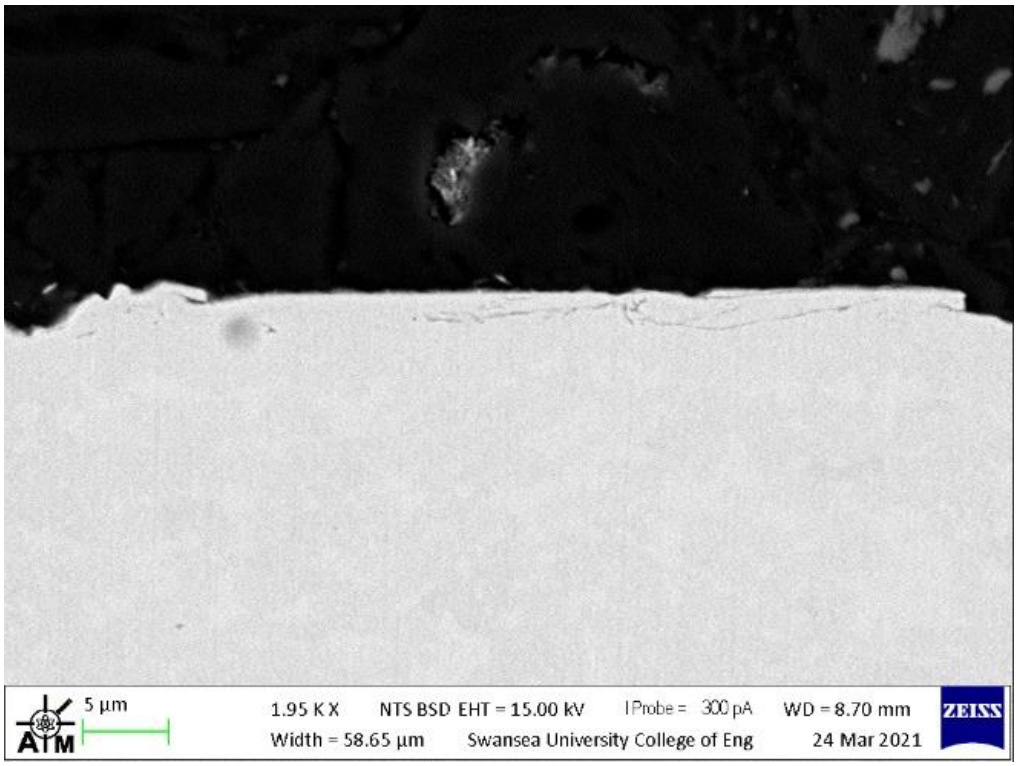

Figure 12: Backscatter imaging of the cross section of C9321101.

As shown by *Figure 12*, the C9321101 has an oxide layer that is located between the substrate and the encasing Bakelite. The steel substrate (light grey) is located at the bottom of the image with the encasing Bakelite above it. Backscatter imaging is a popular method for detecting structural differences in materials under investigation, it is also important to note that it does not show the root of the problem. This can be further shown by the difference in brightness as the oxide layer will appear different from the substrate as they have different atomic numbers. The dark line below the surface is evidence of subsurface oxidation, as this occurs along the grain boundary [3]. This form of analysis can be further consolidated by carrying out quantitative analysis to initially identify the elements responsible (EDS) then phases/oxides (XPS) responsible for this difference in appearance. As illustrated in *Figure 12* and *Figure 13*, there was no distinguishable appearances (both SEI and BSE detectors) on the surface of the sample, even at high magnifications (µm).

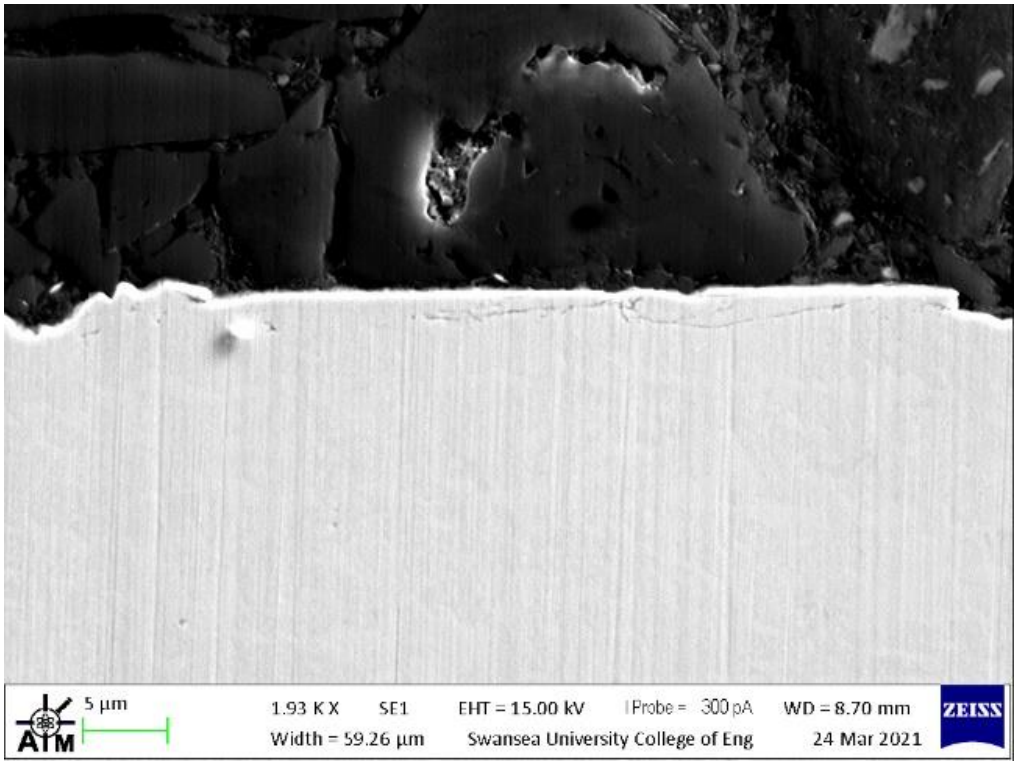

Figure 13: Cross-section scanning electron image of C9321101 and the Bakelite.

4.3.EDS

The sample working distance was 10mm, the EHT voltage was 15kV with a probe current of 300pA and the dead time range was kept between 30-50%. It is important that attention be paid to the dead time as it detects the amount of data that is accepted and that which is rejected as an incident x-ray must arrive after the predecessor has been processed.

Figure 14 is the composition of the elements (the elemental density) by illustrating the brightness of a certain colour relating to that element e.g., Bakelite has a high Carbon content so therefore the detected Carbon signal is brightest in that region, the same applies for Fe. The presence of other elements can be related to the sample preparation i.e., the grinding papers are made from Si. The main distinction is that except for Al the distribution of appears even throughout the sample and therefore if an oxide layer was present, it was not prominent enough to be detected at a magnification (µm) of ×1950. EDS results are proportional to weight percentage, therefore quantitative estimates for Oxygen cannot be reliable through direct measurement of the Oxygen peak with EDS. Since Oxygen is a relatively light and the samples had been exposed to air, the sensitivity of this analysis technique cannot reliably quantify even as an estimate[33].

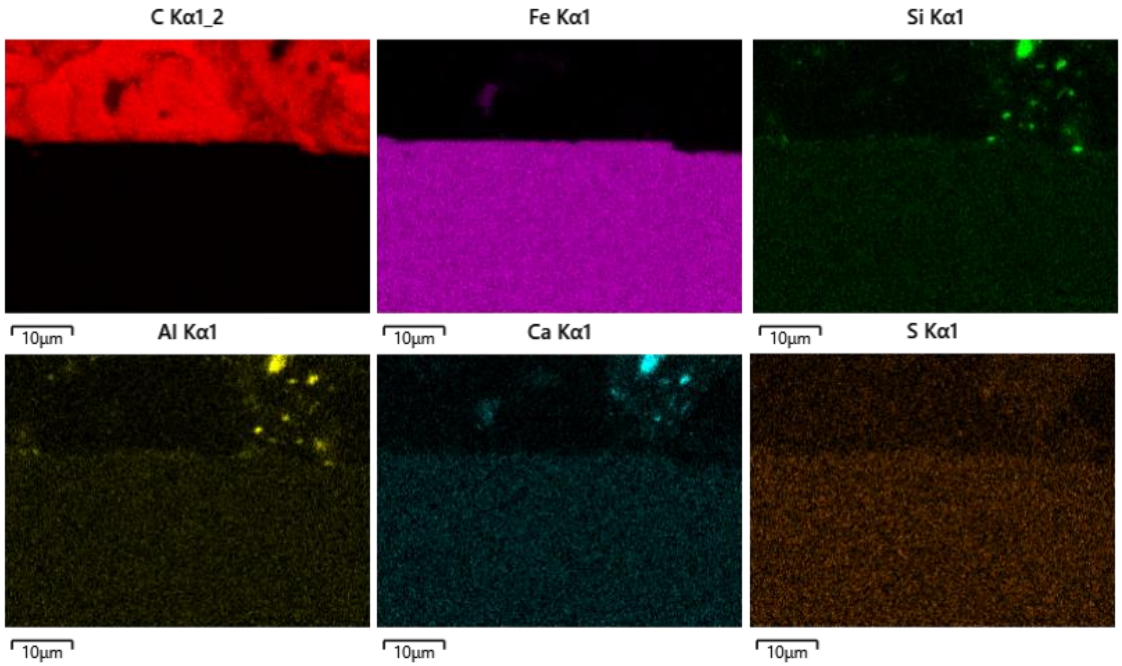

Figure 14:Area map for C9321101 using the reference image from Figure 12 to show the location of certain elements on the sample.

Figure 15 is a map sum spectrum of the cross-sectional area of C9321101 shown in Figure 13. The σ symbol in the table is the deviation which is a measure of the wt% of the elements detected. For elements such as Si, Al, Ca, and S this allows us to reliably conclude their presence despite the small values as the deviation (σ) is zero. A spectrum analysis was also carried out to investigate whether there was any noticeable difference between the internal steel and surface of the substrate. As expected Figure 15 shows the highest weight percentages correspond with the elements most abundant in the Bakelite (C) and the steel (Fe).

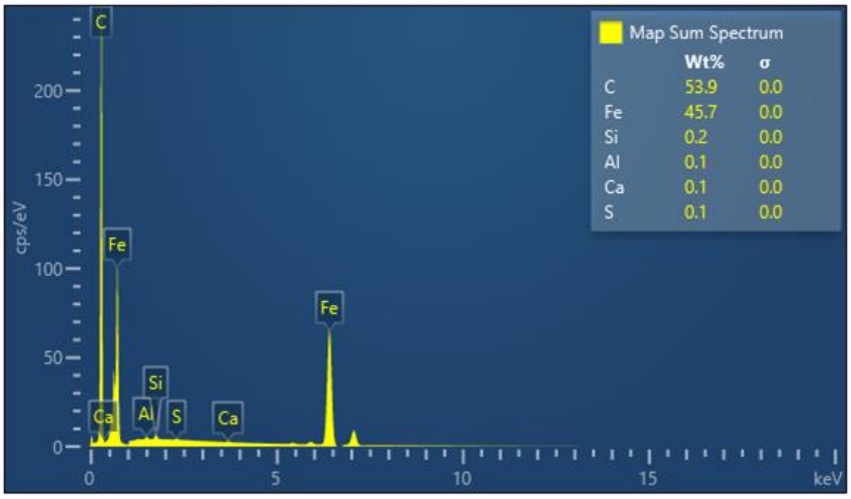

Figure 15: Map sum spectrum of the area where EDS was carried out in Figure 13.

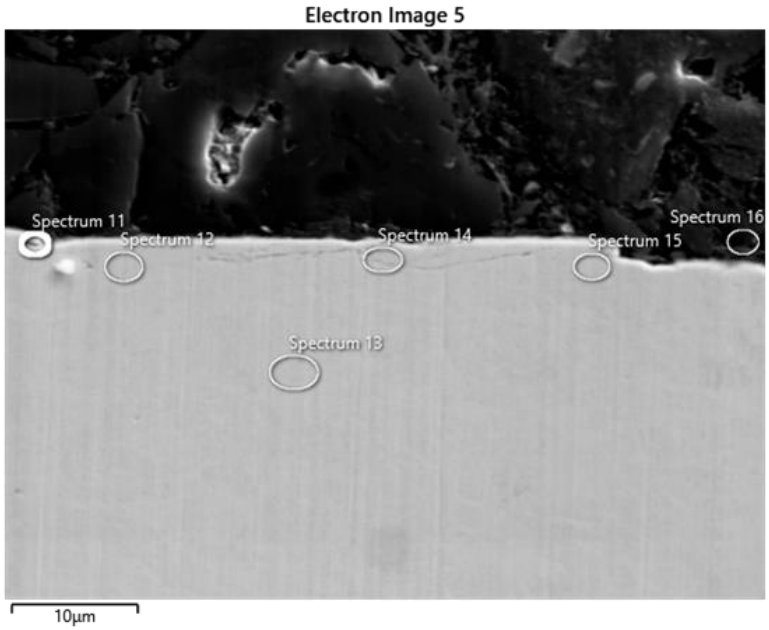

Figure 16*: Point EDS spectrum measurements taken on the cross-section image shown in Figure 13.*

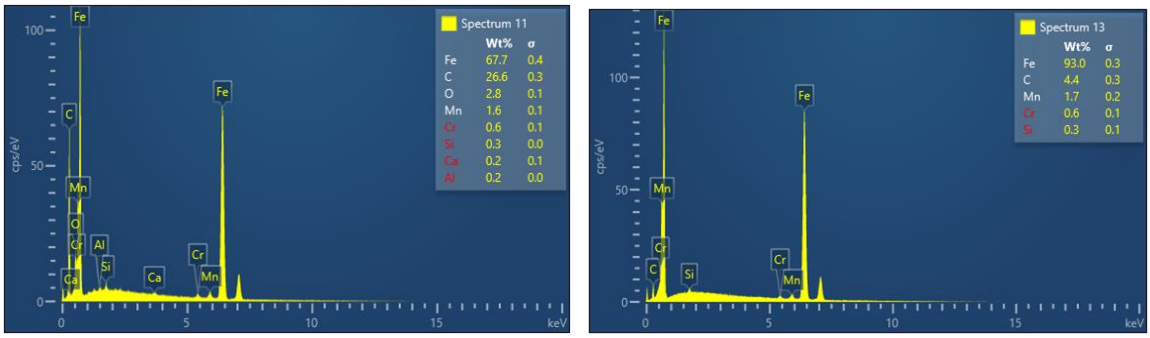

Figure 17*: EDS spectra: (L) Compositional data for spectrum 11, positioned close to the surface of the sample. (R) Compositional data for Spectrum 13, a location deep within the substrate as shown in* Figure 16.

The data in Figure *17*, shows the wt% of the elements in C9321101, spectrum 11 does show the presence of Oxygen, however due to the small atomic number, a more reliable analysis technique will have to be used for verification. The other spectra; 12,14 and 15 had lower values with regards to the wt% of Oxygen. Due to the different locations of the spectra, this allows a distinction to be made with regards to composition for cross section of the interface (where the oxide layer is situated) and the internal of the steel.

4.4.XPS

XPS results were obtained using Kratos Axis Supra XPS (shown below in Figure 18), this equipment using a monochromated Al Kα and achromatic Mg Kα X-ray sources, using classic concentric hemispherical analyser routinely[34].

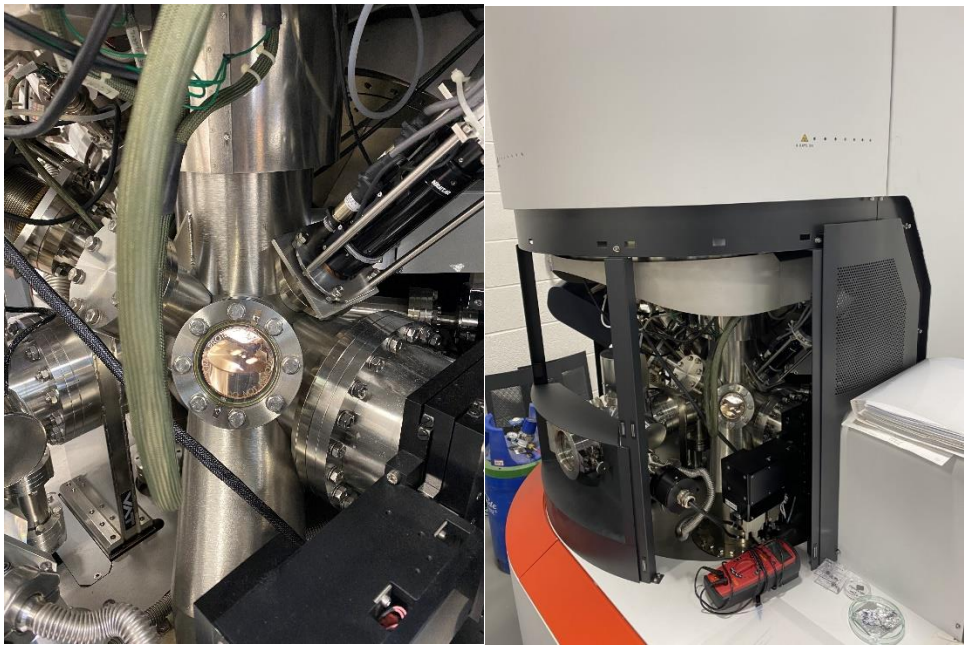

Figure 18: (L) The internal setup of the Kratos XPS equipment, (R) is the external of the equipment used.

XPS was carried out at random points across the sample surface to assess whether there was a difference in composition despite the visual appearance. The spots with the highest counts were chosen for the results. The results showed that in the case of the oxide layer this was not even as the counts per second (CPS) ranged from 500-2000. The distinguishable peaks were as follows: Oxygen (O1s), Carbon (C1s), Fluorine (F1s), Tin (Sn3d), Nitrogen (N1s), Silicon (Si2p), Iron (Fe2p), Manganese (Mn2p), Chromium (Cr2p), Calcium (Ca2p). These were identified using the CasaXPS library and the XPSSimplified online database. Initially using the data bank from CasaXPS higher concentration elements can be identified from the peaks on the survey spectra, lower concentrations are identified by isolating the regions where they may be located and fitting a model peak onto the spectra and quantifying the different phases to conclude whether you can reliably establish the presence of the element or not.

The results show the binding energy (eV) (x-axis) plotted against the counts per second (CPS) y-axis. Due to the unique nature of the binding energy for each phase of the alloying elements this can be used to identify the presence of certain phases using peak positions. It is also

important to note that there will also be an overlap in the binding energy for certain elements, therefore it is also important to have knowledge of the pre-existing chemical structure of the sample. In this case the compositional properties are provided by the manufacturer and EDS is also complimentary as it helped distinguish the elements present. The detection of elements is done through the analysis of peaks and cross referencing the binding energy to the sample library to help determine the samples with the high counts per second (peak fitting). It is also important to note that the method of storage could also be a course of contamination, in this case the presence of C could be because of storing the samples in plastic bags.

To quantify the elements on the surface, using the CasaXPS software, firstly you identify the elements through the binding energy, isolate the region, then create several components correlating to the number of peaks observed. Fitting the components to the regions allows you to calculate the percentage atomic concentration. This is the most reliable method since not all electrons emitted would be recorded and these would vary throughout the analysis for each sample i.e., the difference in intensities would affect the background. This is due to the changes in the x-ray gun power output, since this percentage is a representation of the intensities as a percentage (%) i.e., a ratio of intensity to the total electrons measured. The number of peaks to be fitted depends on the chemical composition, this can also be estimated by the known binding energy states for a particular element e.g., Carbon has three common chemical states. The end goal is to minimise the residual standard deviation of the results to ensure the reliability, in cases with high concentrations the standard deviation is high as it is difficult to distinguish from the background.

To improve the reliability of these results given the sensitivity of XPS and the effect contamination can have on the results, analysis was carried out four times on different locations within the C9321101B sample. Unfortunately, due to the time constraints i.e., availability of the instrument, the other samples only had one location to collect results from.

O1s

Two samples were selected, and results were obtained from different locations within the sample to compare the % atomic concentration throughout the surface. The binding energies included in the results are those within the range typical of metal oxides and Carbonates (529-532eV). As shown in Figure 19 there was little difference in the % atomic concentration values (At%) despite the dissimilar surface appearance. The O1s peak position and % atomic concentration for Sample A was 21.5% at 530.40eV compared to the A sample; 530.52eV and 32.74%.

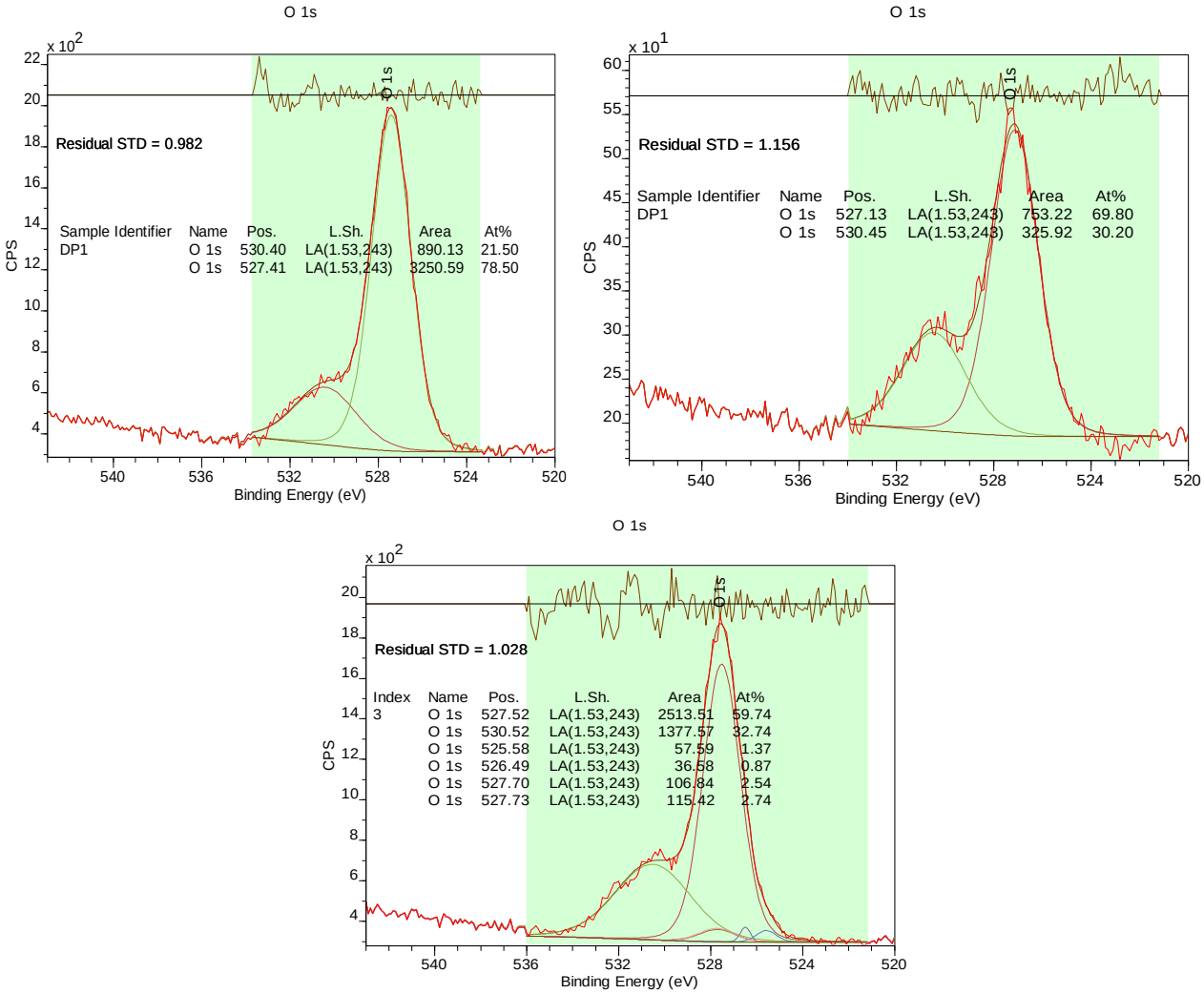

Figure 19: O1s spectra for the C9321101 samples, the left and middle spectra are from the B sample but different scan locations, right side shows the O1s peaks for the A sample.

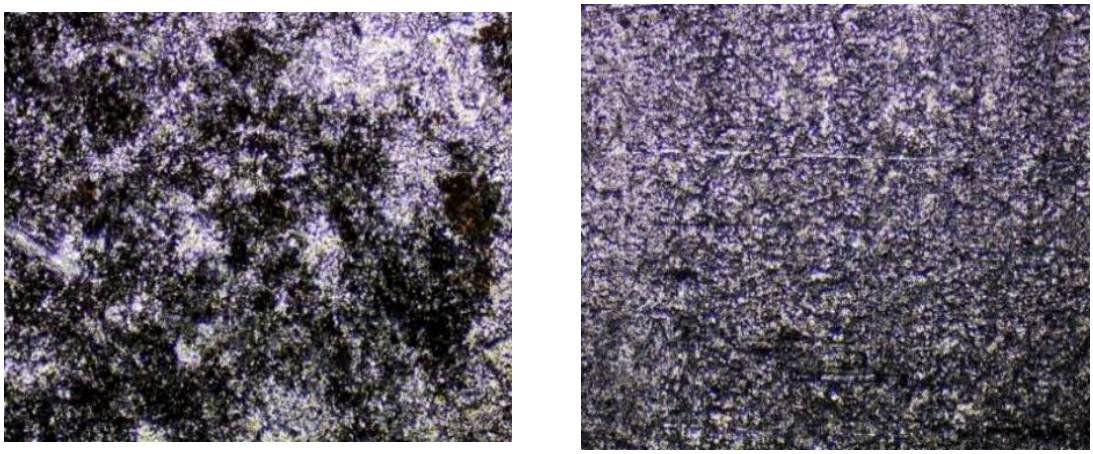

Figure 20:The sample C9321101B (L) that showed discolouration visible as observed through a 5x microscope lens, C9321101A (R) appeared to show no discolouration to the naked eye until observed through a 5x microscope lens.

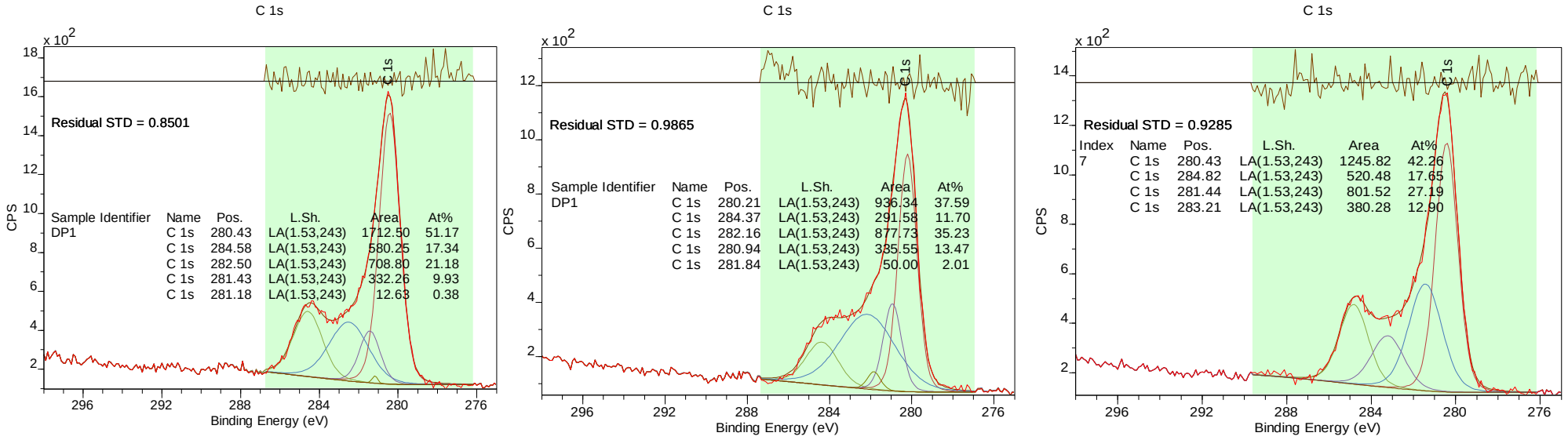

Figure 21: C1s spectra (left and middle) are from two locations on the worst-case, sample B. (Right) spectra is from the best-case, sample A.

C1s

Other elements detected through their corresponding peaks and binding energy included, C1s 284eV, the presence of this element can be because of adventitious Carbon contamination. and the presence of Carbon in steel. The contamination spectrum for C1s typically have the C-C, C-O-C, O-C=O components with binding energies of 284.8eV, ≈286eV and ≈288.5eV respectfully. It is also worth noting that a few nanometres of adventitious Carbon can affect the survey spectrum of the sample. There are also metal fluorides F1s detected on the sample surface, these are shown by the peaks in the 684-685.5eV range. When compared, the concentration between the two samples at ≈284eV, sample B had 284.58eV (17.34%) compared to A's 284.82eV(17.65%), there was no major difference in the atomic concentration at the surface despite the difference in appearance.

Sn3d

For the Sn3d, due to the very similar binding energies of the Tin oxides, SnO 486eV and SnO_2 486.6eV, a valence band spectrum will have to be collected to quantify these oxides using XPS. Figure 22 is the valence spectra of SnO_2 and SnO.

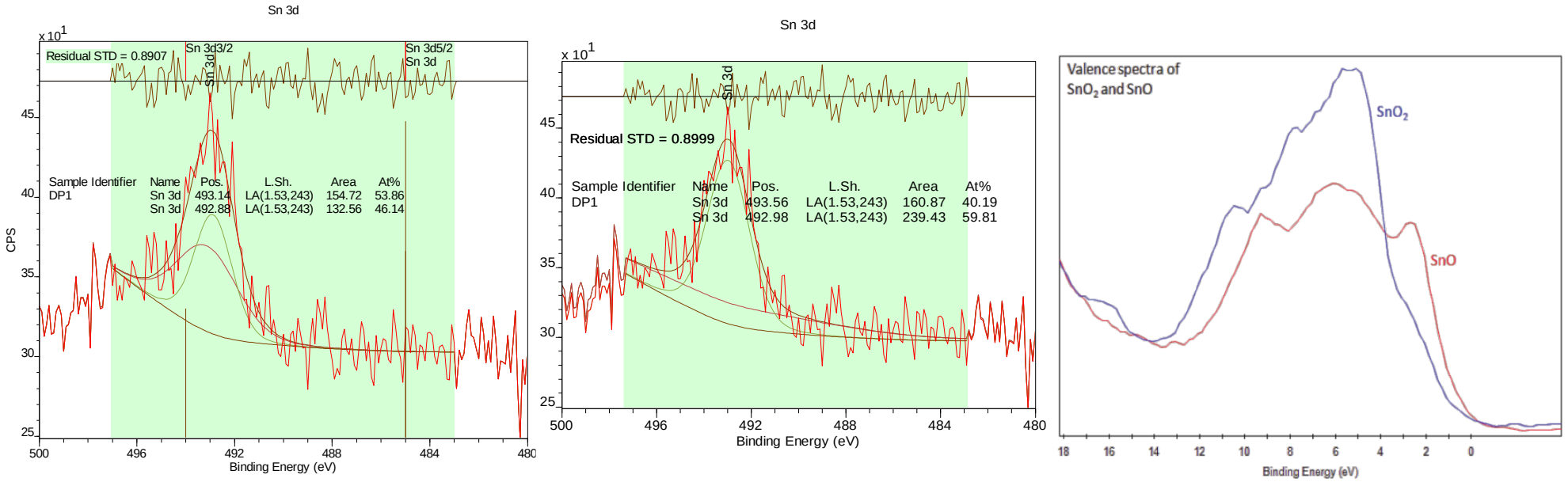

Figure 22: The Sn3d spectra for the surface of the B sample (left) compared to that of the A sample (middle) the valence spectra is on the (right).

The typical binding energy for the tin (Sn) oxides is 486eV, however both samples had similar peak shapes at the same binding energy this can possibly be attributed to the shift[35]. There is a slight difference between the samples with regards to the percentage atomic concentrationn; sample B has 53.86% whereas A has a 40.19% for a similar binding energy (≈493eV, then for the lower binding energy (≈492eV), sample B has 46.14% compared to A's 59.81%.

N1s

Nitrogen is effective in improving the mechanical properties and improving the resistance to corrosion if in solid solution or precipitates i.e., nitrides ≈ 397eV. For the N1s spectra, it is important to note that this region overlap with Molybdenum (Mo), therefore it is important that the region with the binding energy for both Mo3p and N1s is collected (370-455eV). Oxidation normally moves components to higher binding energy; therefore it is important to note the peak shapes for metal nitrides are typically complex and unusual especially given the presence of surface oxynitrides[36].

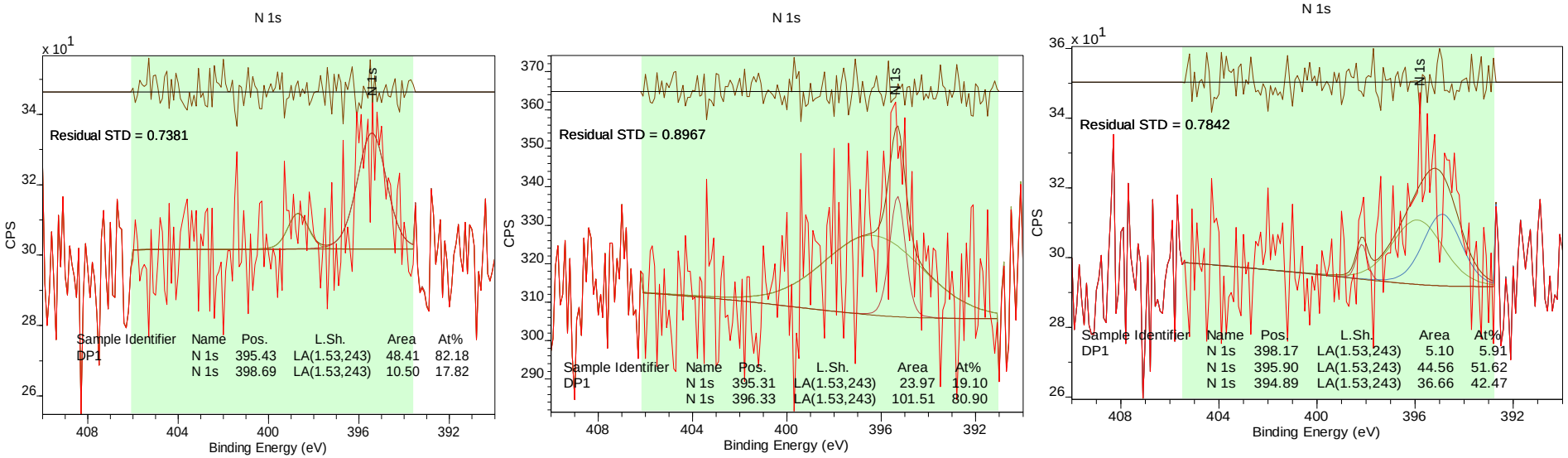

Figure 23: N1s spectra; (left) and (middle) were obtained from the B sample whilst the spectrum on the (right) is that of the A sample.

One peak on both samples' spectra corresponded with the binding energy typical of metal nitrides (≈397eV, with B sample's 398.69eV and A's 398.17eV) despite the relatively low percentage atomic concentration (17.82% and 5.91%) respectively.

Si2p

Analysis of the Si2p spectra showed a single distinctive peak region for the first sample which is common for Si in its elemental form. Sample A showed the most distinct peak within the binding energy of Aluminusilicates (102.49eV) with an atomic concentration of 13.25%, B samples did not have any distinct peaks above 100eV indicating a distinct difference in the surface chemistry. The reliability of these results can be improved by carrying out multiple readings for the B sample to evaluate the reliability of these measurements.

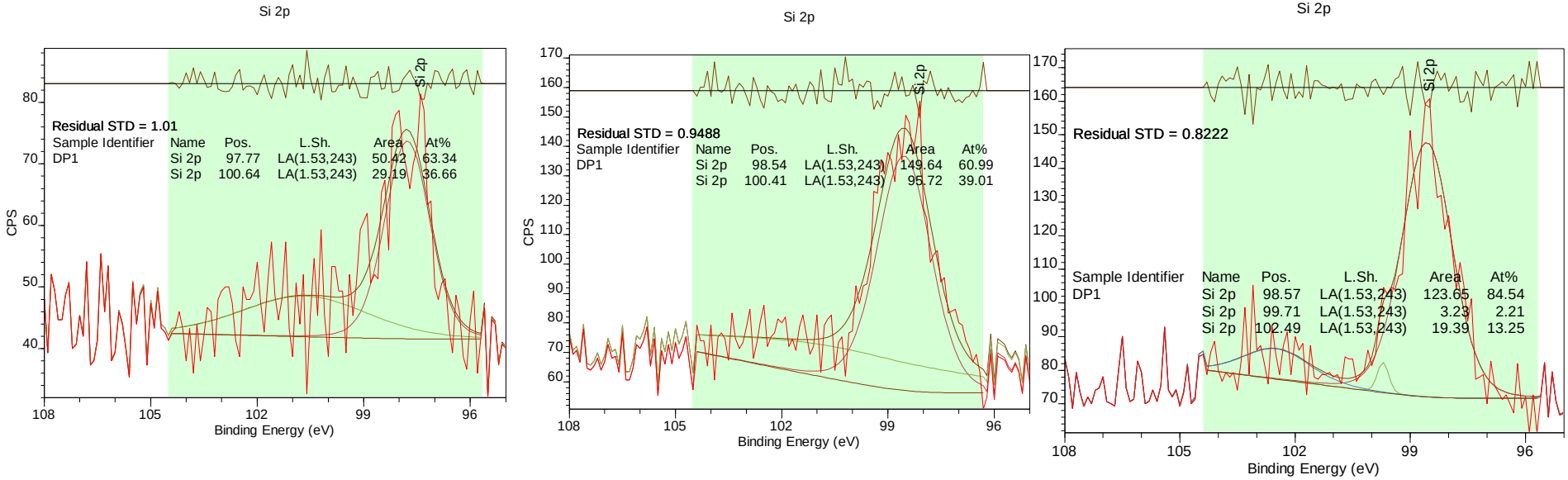

Figure 24: Si2p spectra; sample B spectra are (left) and (middle), sample A's spectrum (right).

Fe 2p

FeO and Fe_2O_3 have binding energies of 709.6eV and 7210.8eV, therefore, to distinguish the oxidation state of the metal when determining the oxide formed, the satellite spectra in Figure 26 are used as reference. As illustrated in Figure 25, both samples have a high concentration of Fe metal 706.7eV (46.24% and 76.06%) for the B samples and 15.83% for the A sample, which is to be expected given the abundance of iron within steel. However, the A sample has a higher concentration of iron oxide (61.47% + 22.70%) compared to that of B samples' (53.76% and 23.94%).

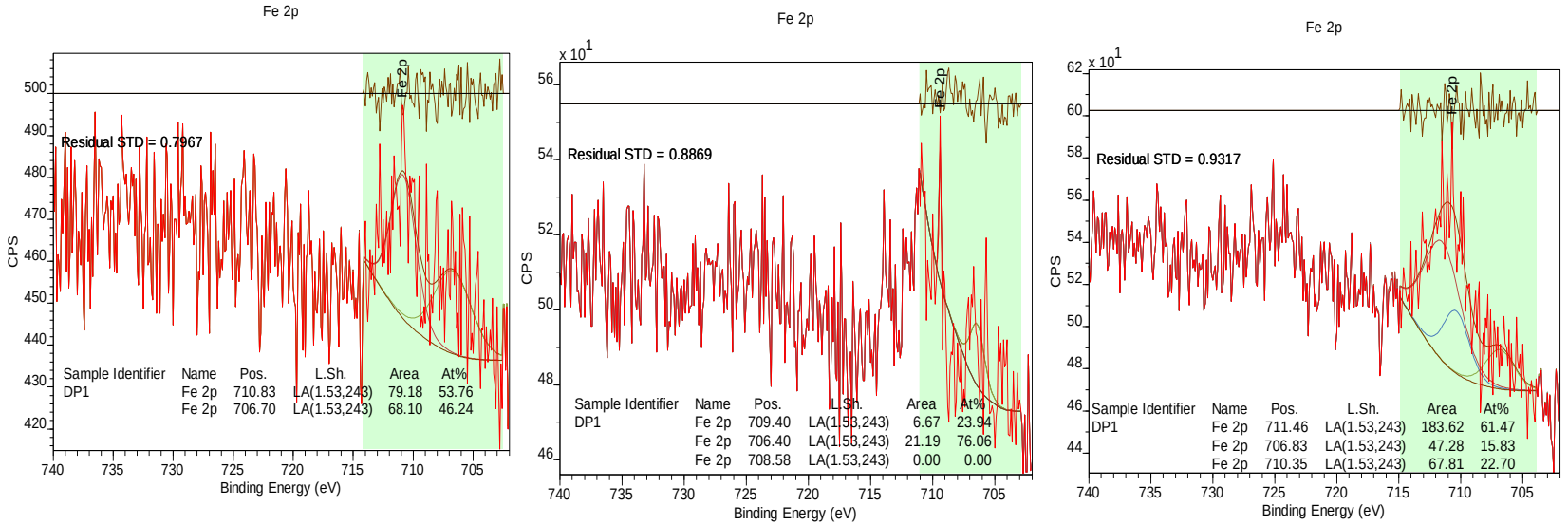

Figure 25: Fe2p spectra: Sample B spectra are (left) and (middle) whereas sample A's spectrum is located on the right.

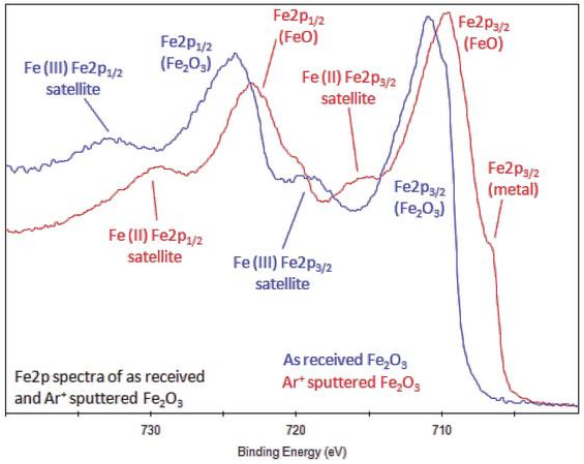

Figure 26: Satellite features that be used to distinguish the different oxidation states of Fe2p [37].

Mn2p

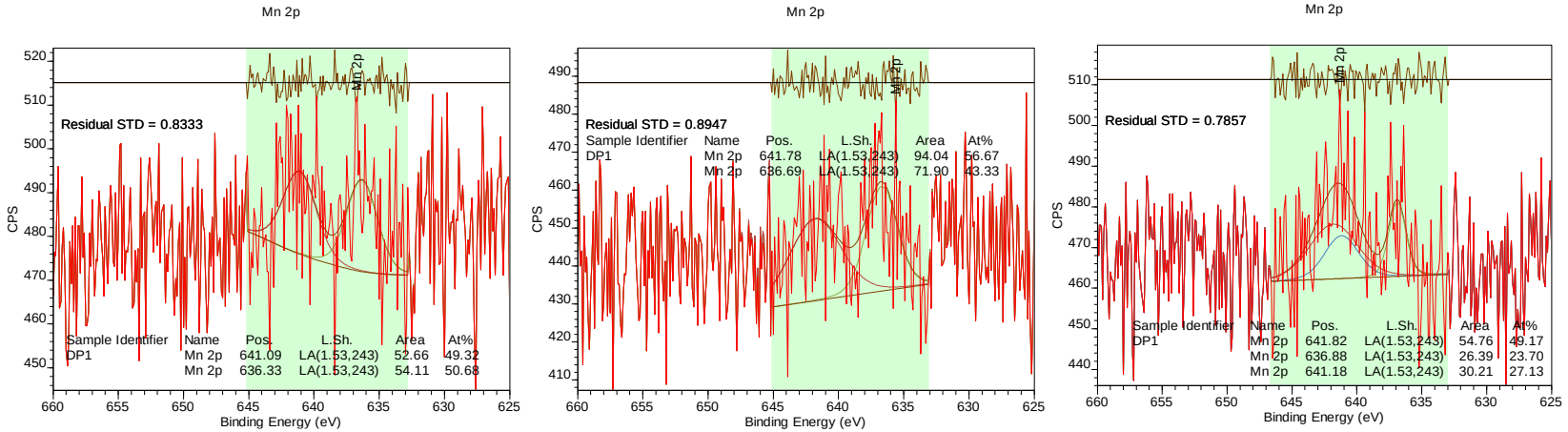

Figure 27:Mn2p Spectra; of Sample B spectra (left) and (middle), sample A's spectrum is shown on the (right).

For Mn2p, it is important to note that for this primary region, MnO and Mn_2O_3 have the same binding energy of 641.4eV and 641.8eV respectively. Mn oxide peaks are significantly shifted to higher energy than the metal. B samples have a lower atomic concentration of Mn oxides (binding energy ≈641eV) 49.32% and 56.67% compared to that of the B sample 49.17% and 27.13%.

Cr2p

The spectra for both samples did not have peaks as defined for the Cr2p spectra, this is possibly due to the strong overlap with Zn LMM Auger peaks, is the Chromium concentration was high enough Cr3p spectra would have been the preferred option. The binding energy ≈574.3eV indicate the presence of Cr metal on the surface (46.07at%). Figure 28 shows both sample A and B had second peaks at binding energies >580eV indicate the potential presence of a Cr (VI) oxide, sample B middle spectra also showed a peak at a binding energy like that of the Cr (III) oxide (≈576eV) with 78.78at%.

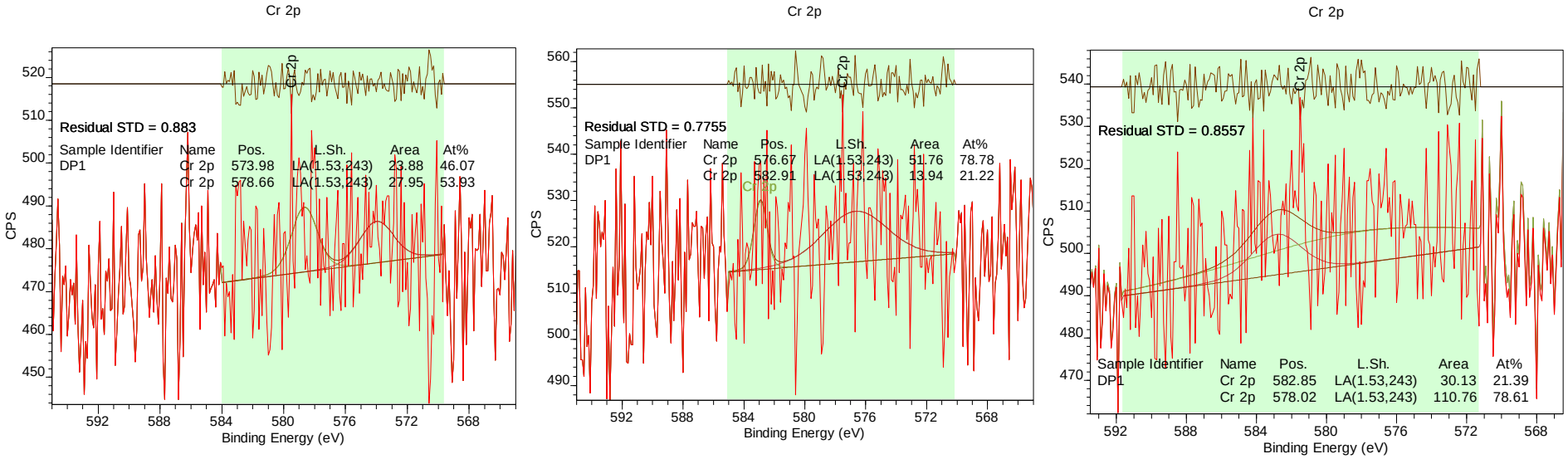

Figure 28:Cr2p spectra; Sample B spectra (left) and (middle), sample A spectrum is on the (right).

Ca(2p)

Due to the highly reactive nature of Ca metal, it is always present as a compound. Both B and A samples showed the satellite features and the two distinct peaks. As shown in Figure 29, all samples showed similar spectra shape with peaks occurring in similar locations, there was very little difference with regards to the at% within these binding energies.

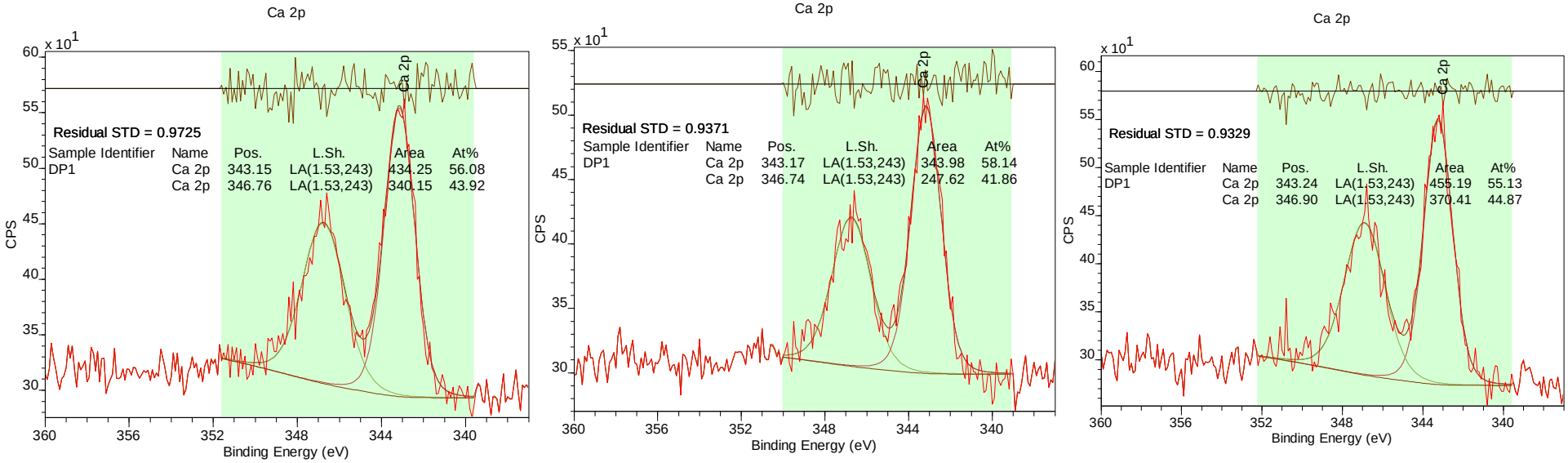

Figure 29: Ca2p spectra; (left) and (middle) spectra are obtained from the B sample, the (right) spectrum is from the A sample.

4.5.TalySurf

All samples released by the manufacturer have to meet the release criteria for the roughness parameters, therefore the disctinction this method of characterisation seeks to establish is the extent surface appearance has on roughness. Therefore two samples were taken from each of the specimen analysed and a comparison was made between the values. Three line measurements were carried out on each sample to observe the numerical difference between the values for the samples deemed OK and NOK.

There were no major differences in the average roughness (Ra), the root mean square (RMS) (Rq=Rrms), profile maximum height above mean line (Rp), maximum depth below the mean line (Rv). The B sample had slightly bigger values for the local maximum height (Rmax) and the average maximum at multiple sample lengths (Rz) which is less susceptible to scratching. A predominantly negative Rsk value, which is a measure of symmetry means that the samples had predominantly holes on their surface.

Table 4: TalySurf results for C9321101 sample, showing the values for the A and B samples.

Sample Name		**Ra**	**Rq**	**Rp**	**Rv**	**Rt**	**Rmax**	**Rz**	**Rrms**	**Rsk**
C9321101A	**1**	0.885	1.08	2.38	2.83	7.27	6.55	5.21	1.08	-0.151
	2	0.922	1.1	2.21	2.91	6.54	6.33	5.12	1.1	-0.102
	3	0.816	0.992	1.95	2.86	8.38	5.67	4.8	0.992	-0.209
C9321101B	**4**	**0.789**	**0.94**	**2.04**	**2.26**	**5.01**	**5.19**	**4.3**	**0.94**	**-0.0535**
	5	**0.737**	**0.889**	**1.84**	**2.63**	**5.79**	**5.33**	**4.47**	**0.889**	**-0.113**
	6	**0.843**	**1.01**	**2.24**	**2.56**	**7.66**	**6.36**	**4.79**	**1.01**	**-0.0446**

1-3 correspond to the three readings taken of the DP1000A sample, whilst 4-6 are the readings from the B sample. These samples were selected based on their surface appearance as illustrated in

Given the values presented in the table, the surface appearance does not seem to adversely affect any of the values in a distinctive way, this is largely in part due to the samples having to meet the roughness parameters for the release criteria therefore deviation is very minimal. The sample seems to indicate several single peaks since the **Rt>Rz**.

4.6.C9321101 (DP1000) Summary of Results

- No visible oxide layer using SEM at high magnification (µm) using scanning electron (SE) at 1950x and backscatter diffraction (BSE) at 1930x
- EDS showed that the corresponding elements within the sample and the Bakelite.
- XPS showed that despite the observable difference in appearance, there was very minimal differences in the % atomic concentration for the **O1s** spectra, and the shape of both the A and the B sample spectra were similar with very little distinguishable features.

4.7.C7025701 and 6491201 (DP800)

Surface Appearance

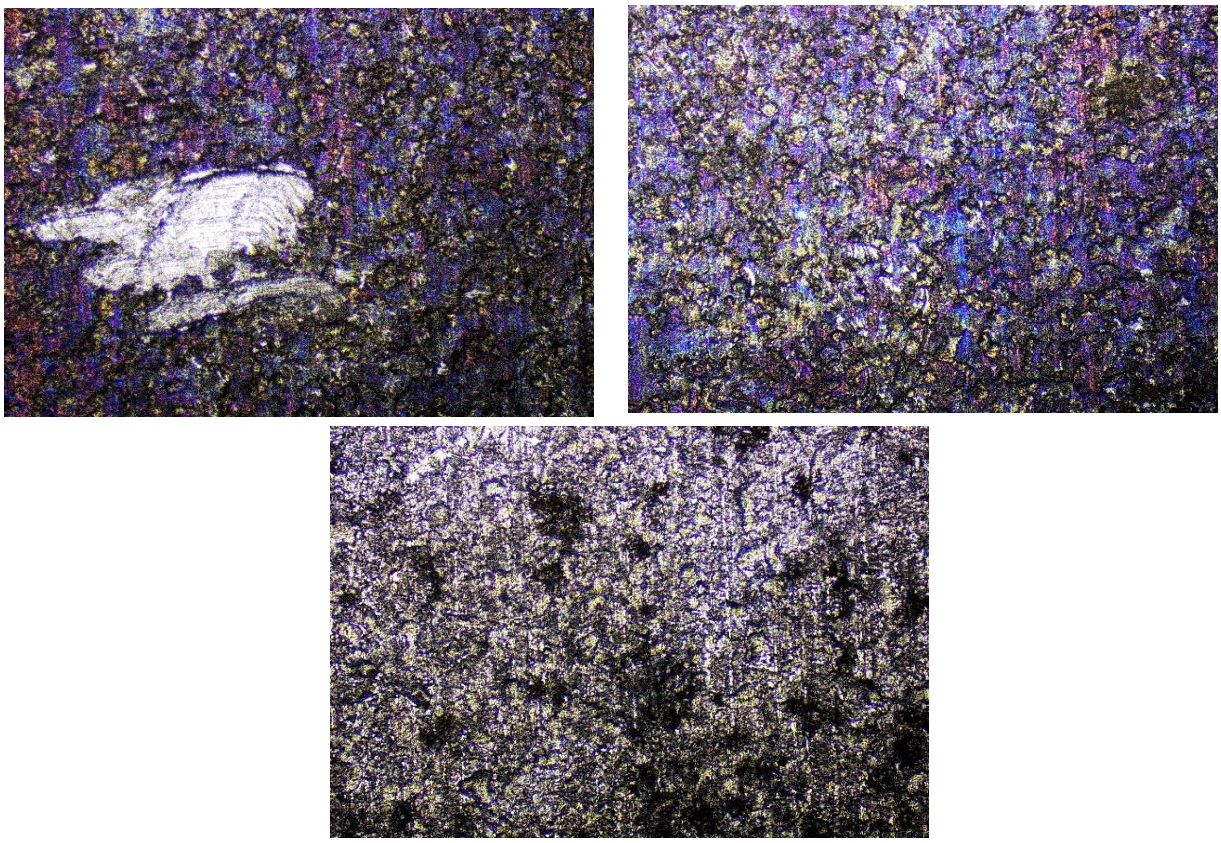

Figure 30: 6491201 edge samples E1 (left) and E2 (right) show the blue discolouration on the surface responsible for the dark appearance, the C7025701 D1A sample on the (bottom) in contrast has a darker grey/black discolouration

As observed in Figure 30, when observed through a 5x lens, the 6491201 edge samples 1 and 2 showed blue discolouration, which was consistent with what had been observed visually. The C7025701 D1A sample however, showed a darker surface discolouration and the level of discolouration was not as extensive as that in the edge samples of the 6491201 sample.

4.1.SEM and EDS

The boundary between the Bakelite and the cross section of the mounted sample, the contrast along the boundary of the samples shown in *Figure 31*, indicates the presence of an oxide layer. It is also important to note that this is at a very high magnification (µm), therefore though it is present this oxide layer is very small hence the relatively shiny appearance of the sample (no visible discolouration).

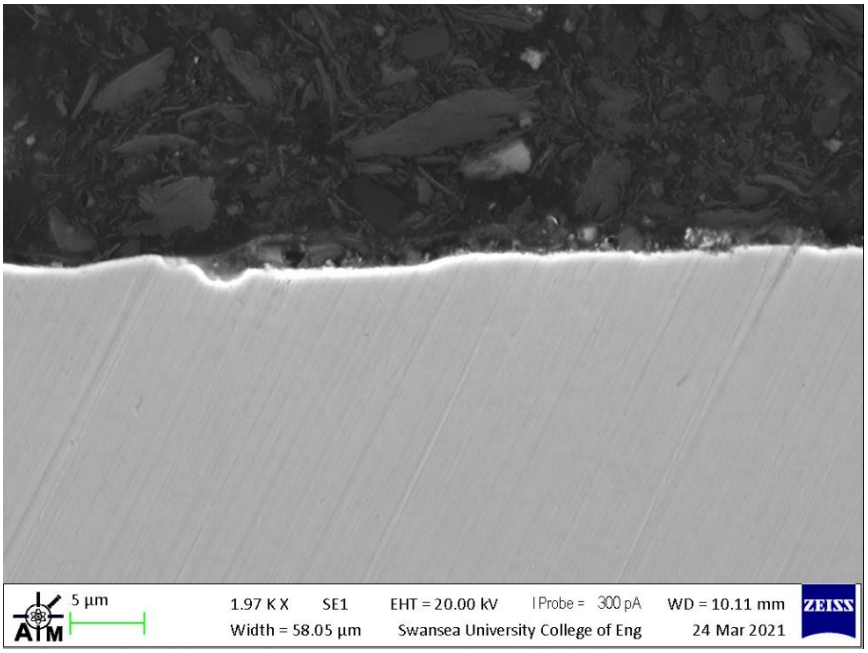

Figure 31: SEM image of the cross-sectional surface of the 6491201 E1 sample.

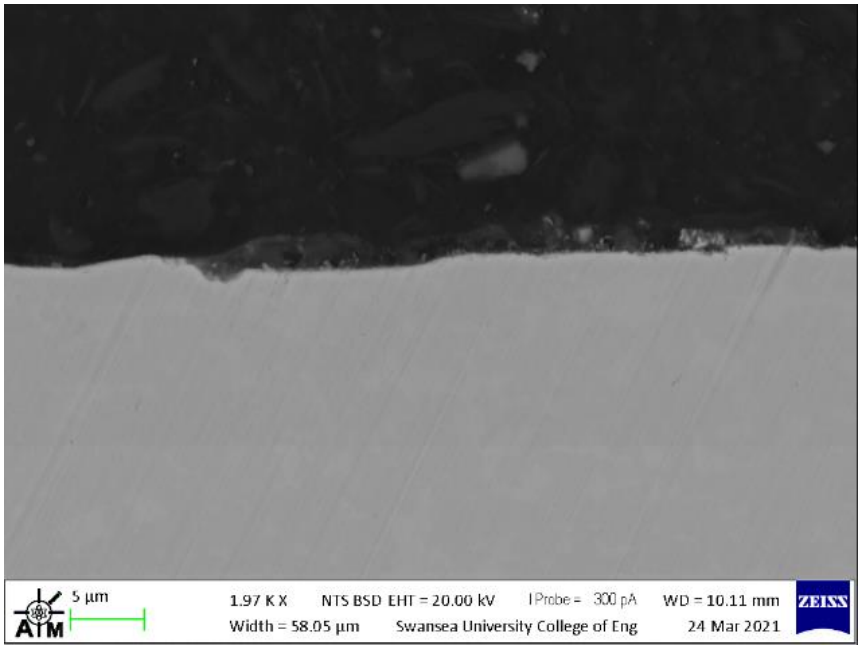

Figure 32: BSE scan of the sample with an oxide layer present on the surface of the 6491201 E1 sample.

Unlike the scanning electron image (SEI) the BSE as shown in *Figure 32* does not seem to show the distinction between the Bakelite, oxide layer and the substrate. This is because of the size of the oxide layer is minimal therefore the differences in density would not be clearly distinguishable like the image illustrated in Figure 33. Using BSE would have enabled a cross sectional view of any surface oxide as illustrated in Figure 33, which shows the oxide layer on the rusted bumper sample. The difference in the atomic number is the reason why there is a

contrast between the substrate, oxide layer and the Bakelite. Compared to Figure 32 where the oxide layer is not visible even at high magnification (µm).

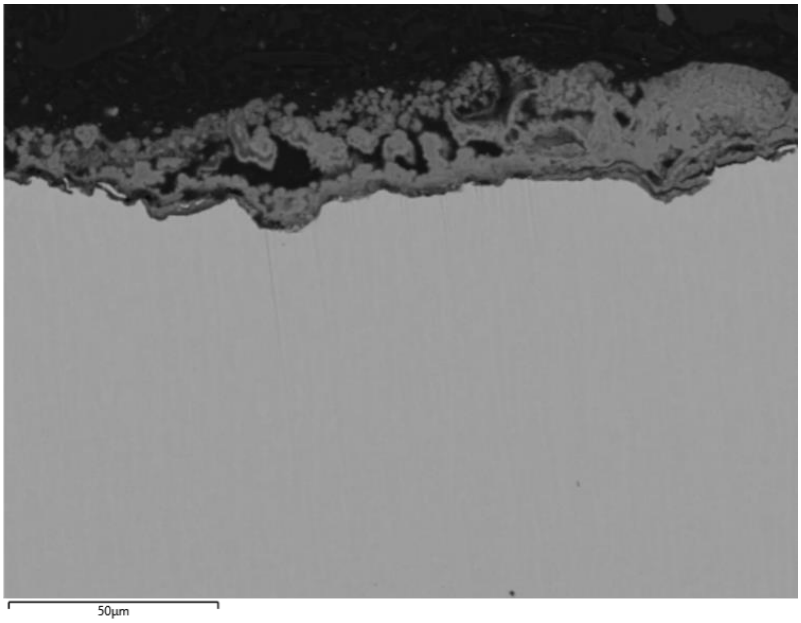

Figure 33:BSE image of a rusted bumper sample, given the difference in electron density between the metal and the iron oxide, they can be distinguished by the difference in shade.

4.2.XPS

For the DP800 samples there were two coils provided with samples E1, E2 (6491201) showed the most discolouration compared to the C7025701 samples. The difference in surface appearance can be attributed to the different annealing atmospheres, the 6491201 samples are thicker in width therefore forming conditions would have differed from the C7025701 coil. All the samples were collected from the edge of the sheets as the E1 and E2 samples were provided prior, therefore, to ensure comparison was reliable, the other samples were cut from the edge of the sheets provided. The blue discolouration for the 6491201 is visible to the naked eye whereas C7025701 is only observable under microscope.

Given the similar compositional range for the DP800 samples, the XPS results can be compared between similar samples from the same coil and the difference between the two coils (6491201 and C7025701). The sample labelled D1 50/50 was the sample where one half showed discolouration while the other showed no discolouration. Using this technique allows the quantification of the elements responsible for the discolouration since all the samples were analysed under similar conditions (they were simultaneously mounted and analysed).

F1s

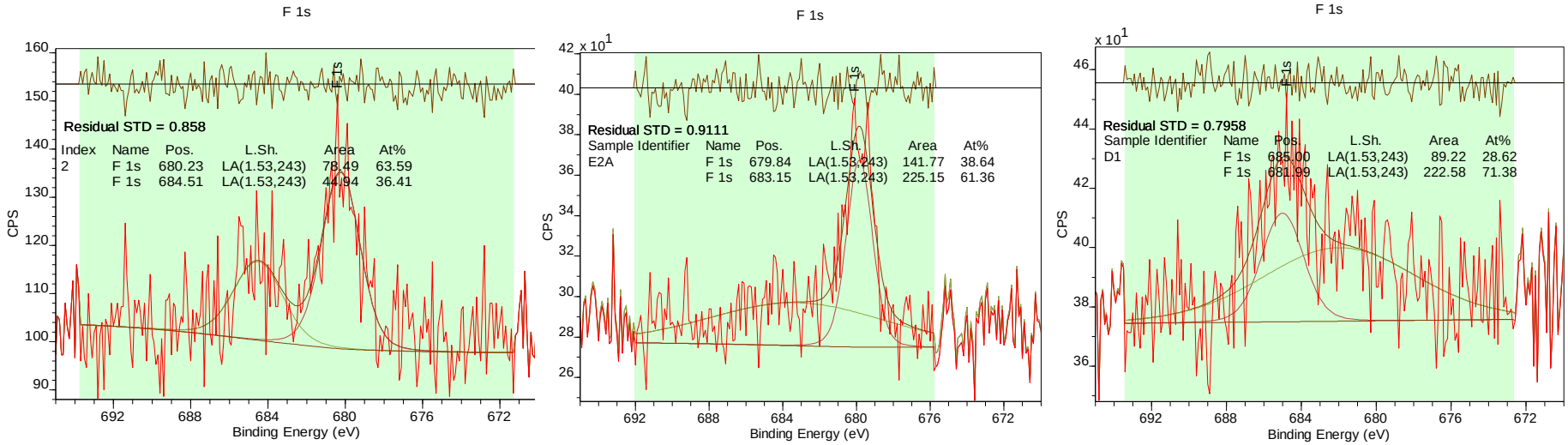

Figure 34: F1s spectra: E1A (left), E2A (middle) and D1A (right).

The spectra for the 6491201 samples showed similar peak shapes around 680eV, the focus however is within the 684-685.5eV range which confirms the presence of metal fluorides. All samples showed a peak within this range with the E1A and E2A samples showing a higher % atomic concentration (36.41% and 61.36% respectively) whilst the C7025701A showed the smallest concentration at 28.62%.

Sn3d

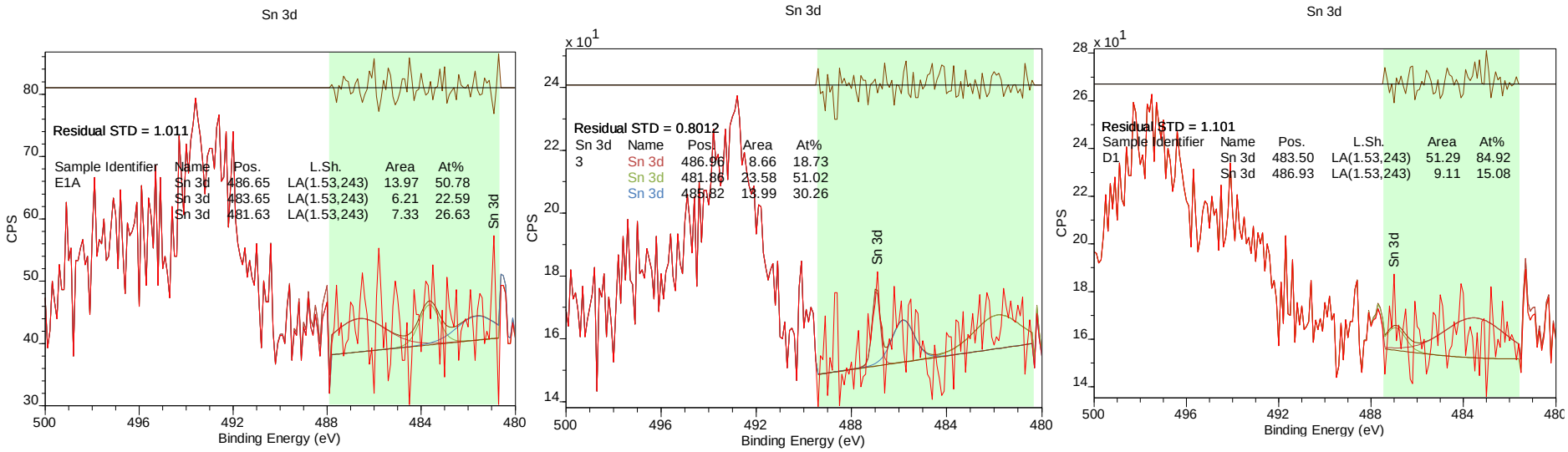

Figure 35:Sn3d spectra: E1A (left), E2A (middle) and the D1A (right).

E1A three distinct peaks with binding energies indicating the presence of an SnO_x on the surface of the sample. E1A had the largest % atomic concentration for the oxide. E2A showed the presence of Sn oxides on the surface represented by the peak at 486.96eV, the concentration was 18.73% and 30.26% of the surface atomic concentration occurred around the binding energy of the Sn metal. D1A on the other hand showed a peak at 483eV like that of E1A but had a very small %atomic concentration for the oxide on the surface.

It is also worth noting that all three samples showed the highest % atomic concentration at binding energies greater than 492eV, with D1A showing a higher CPS count at ≈497eV.

N1s

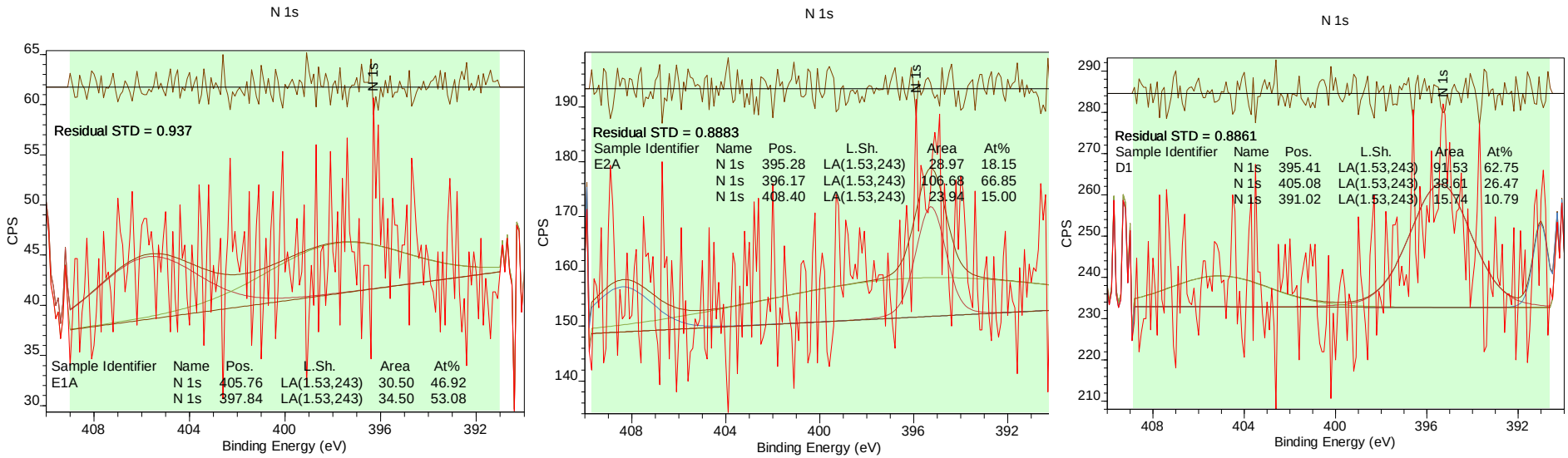

Figure 36: N1s spectra: E1A (left), E2A(middle) and D1A (right)

All samples showed the presence of metal nitrides in high concentration peaks, ≈397eV (E1A = 53.06%, E2A = 66.85% and D1A = 62.75%) this is however to be expected given the annealing atmosphere being rich in Nitrogen.

Si2p

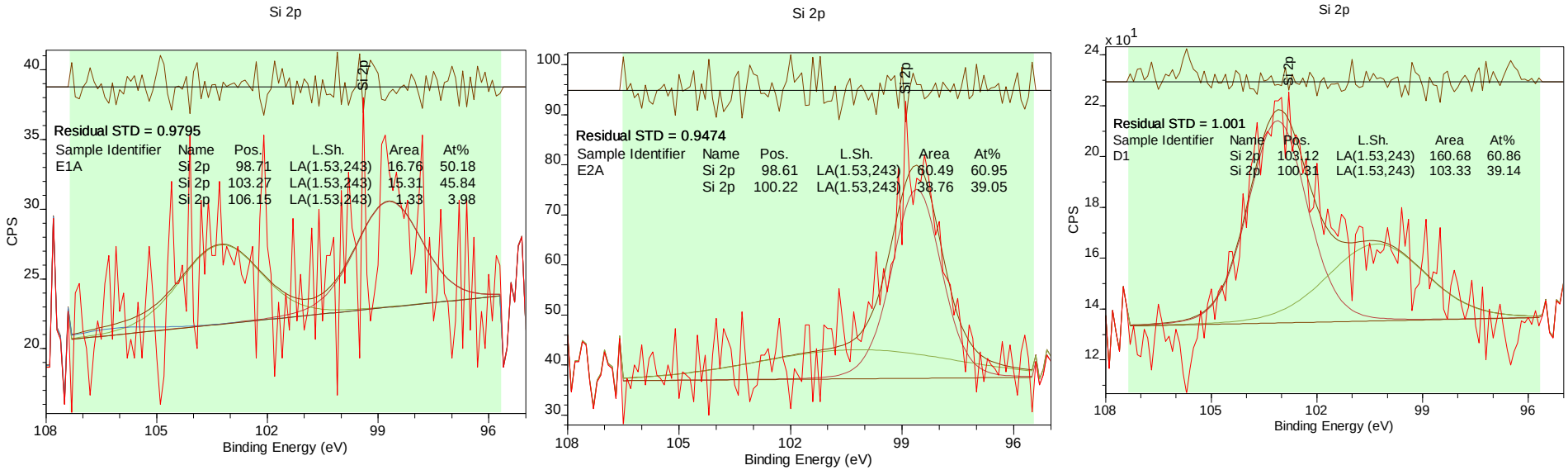

Figure 37: Si2p spectra for E1A (left), E2A (middle) and D1A(right).

Si element has a binding energy of 99.4eV this was the predominant peak position observed in all three samples (E1A = 50.18%, E2A =60.95% and D1A = 39.14%), E1A and D1A showed the presence of Silicon oxides on their surface (103.27eV (45.84%) and 103.12eV (60.86%). Given the multiple peaks within the spectra of all samples, a clear distinction can only be carried out through repeating the analysis, currently only their presence can be confirmed.

O1s

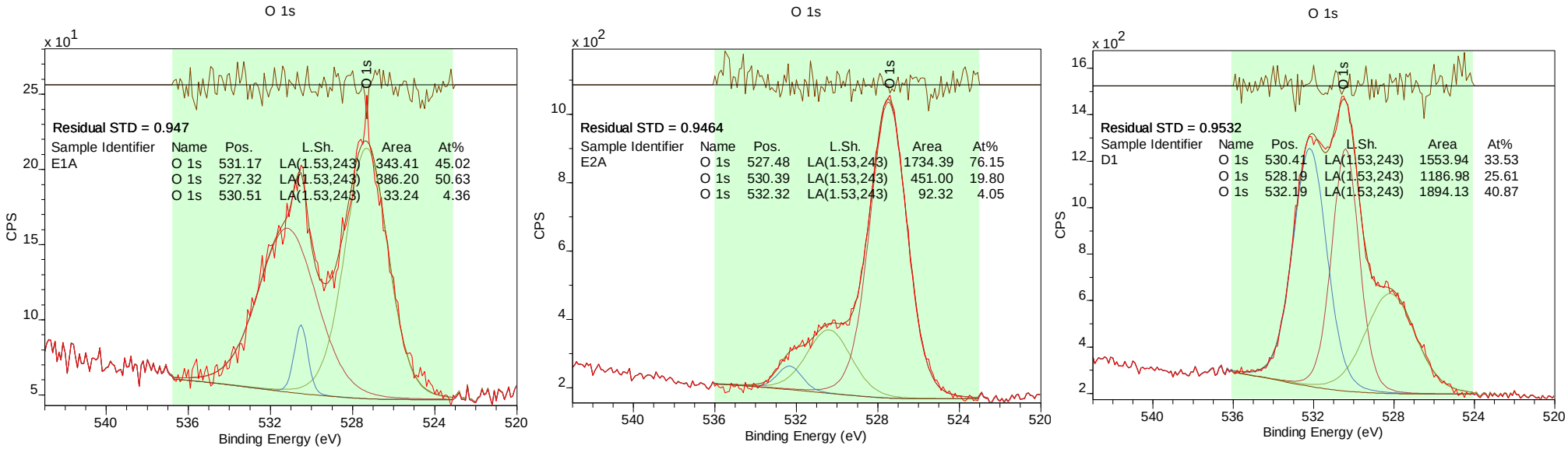

Figure 38: O1s spectra: E1A (left), E2A(middle) and D1A (right).

All three samples had peaks at 530eV, the binding energy for metal oxides, E1 and E2 had smaller % atomic concentration (4.36% and 19.80% respectively) compared to D1A's 33.53%. It is also worth noting that all samples also showed the presence of Alumina (531.1eV) and SiO_2 (532eV) on their surfaces. However, due to sample storage these regions also overlapped with the adventitious Carbon contamination therefore the % atomic concentration would not be entirely representative of just metal oxides being on the surface.

Fe2p

To reduce residual standard deviation, the range for peak fitting was reduced to that where Fe2p3/2 was located as illustrated in Figure 39. To give a more accurate representation from the survey spectrum, both peaks are fitted to show the concentration. The binding energies for the oxides are dependent on whether its Fe2p1/2 or Fe2p3/2.Figure 39: Fe

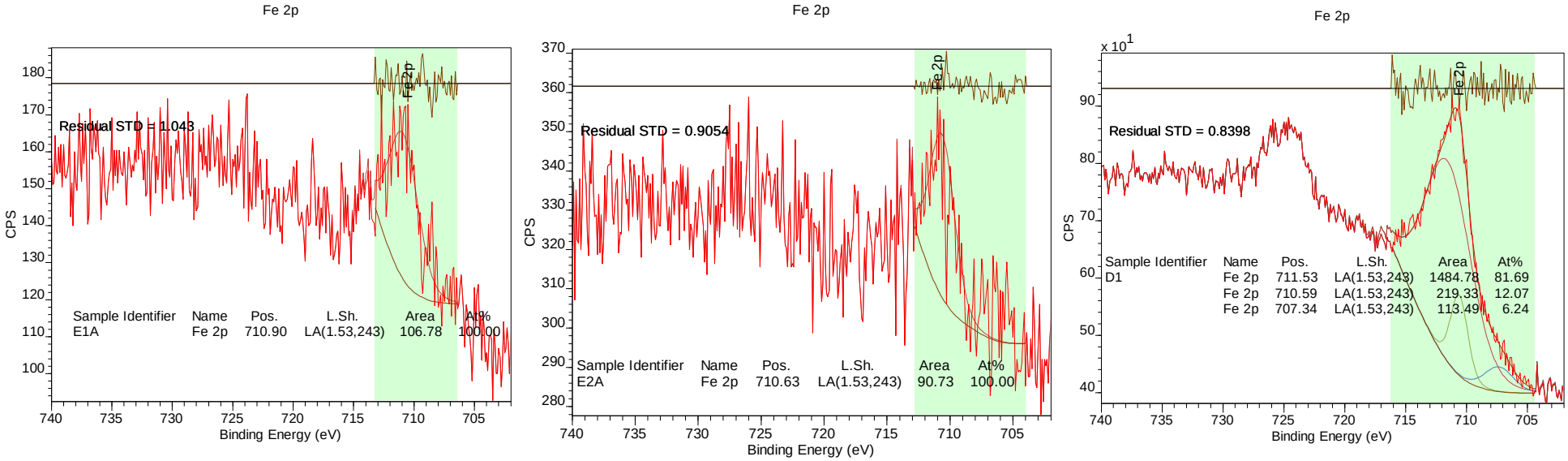

Figure 39: Fe 2p spectra: E1A(left), E2(middle) and D1A (right).

Both E1A and E2A did not show any other distinct peaks besides the singular ones at 710.9a and 710.63eV showing the presence of metal oxides (Fe_2O_3 710.8eV) and potentially chlorides (710.4eV). However, given the noise shown by the spectra of both E samples it is difficult to confidently quantify the level of oxidation, D1 has a clearer spectrum with distinct peak shapes showing the similar peak location 710.59eV showing the presence of metal oxides or potentially chlorides. Given that readings were carried out four times producing similar peak shapes, these % atomic concentrations can be used to quantify the oxidation on the surface of the D1A sample.

Mn2p

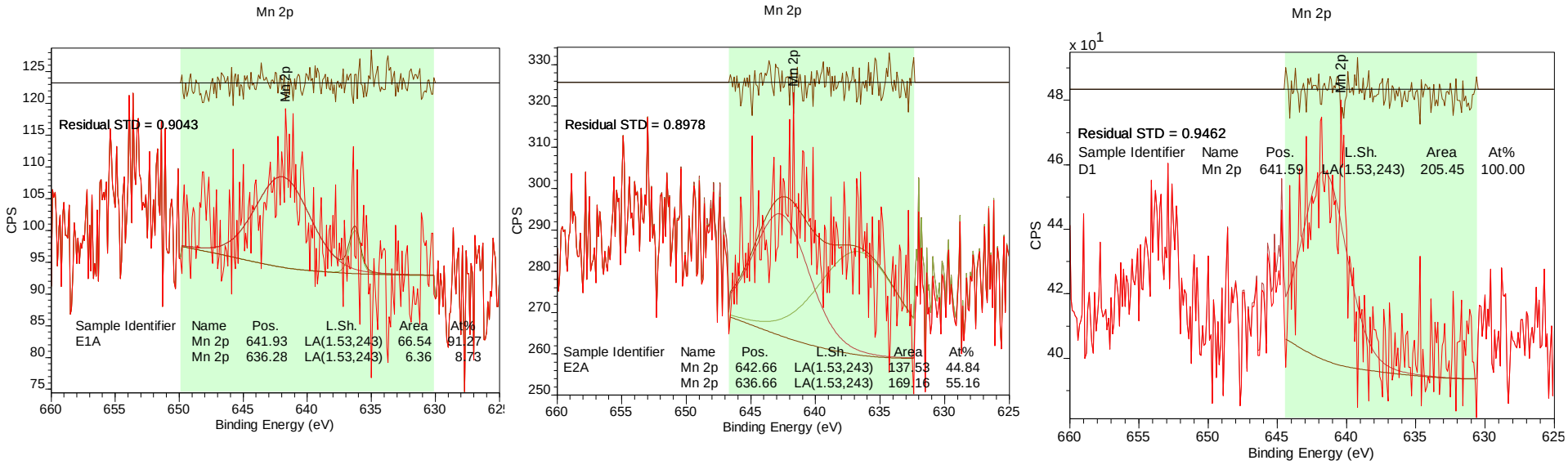

Figure 40: Mn2p spectra: E1A(left), E2A(middle) and D1A (right)

Both E1A and E2A showed double peaks at binding energies of 641.93eV(91.27%), 636.28eV(8.73%) for E1A and 642.66eV(44.84%), 636.66eV(55.16%) for E2A. This confirms the presence of Manganese oxides with high atomic concentrations confirming the original thesis that Mn was to diffuse to the surface due its high Oxygen affinity. D1A showed the same % atomic concentration as the Fe 2p, there was no other distinguishable peaks within the spectra, if reproducible this shows a larger extent of surface oxidation as a result of Mn diffusion.

Due to the overlap for the oxides Mn2p3/2 MnO (641.4eV) and Mn2p1/2 Mn_2O_3, the most reliable way of distinguishing the composition would be to peak fit for both 1/2 and 3/2 to obtain the true concentration of each oxide.

Cr2p

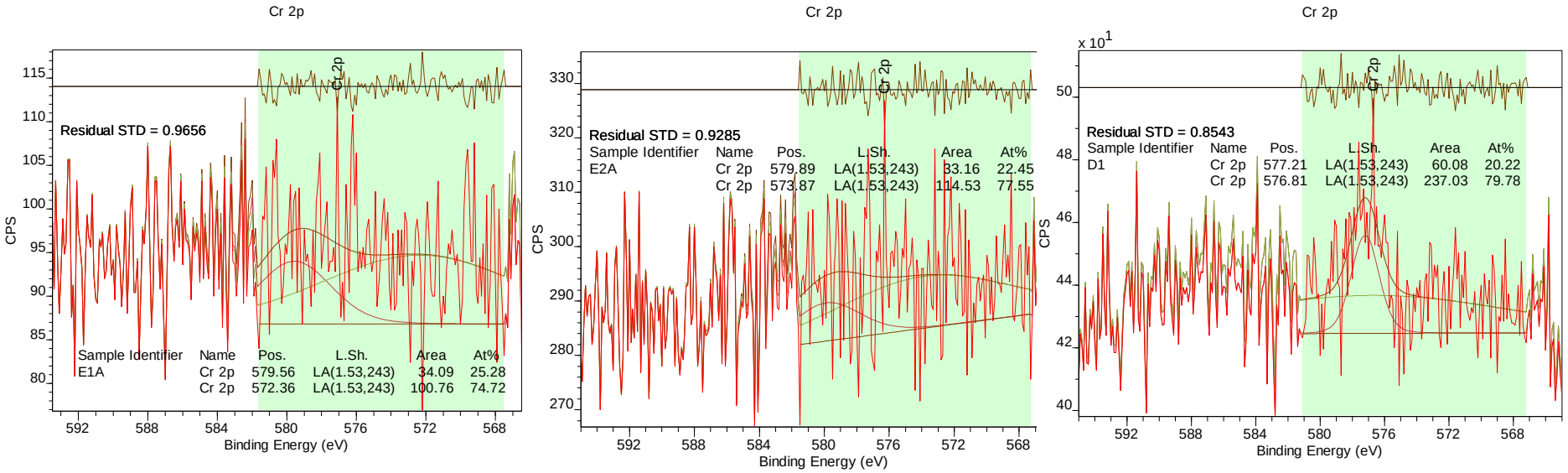

Figure 41: Cr2p spectra: E1A(left), E2A(middle) and D1A (right)

It is important to note that the binding energies for Cr in its elemental form is 574.3eV, as an oxide it is an estimate; Cr (III) oxide ≈576eV and Cr (VI) oxide ≈580eV.

Due to the overlap within steel samples, the spectra for Cr3p are preferable when quantifying the chemical composition of Cr within the sample. The spectra show a peak at the binding energy range for Cr (III) oxide, this trend is observed throughout all the samples analysed.

All three samples had two major peaks, however, samples E1A and E2A had similar binding energy ranges corresponding to both the Cr metal (574.3eV), with both samples having a greater % atomic concentration (74.72% and 77.55%), whereas D1A shows purely oxides on the surface most likely to the Cr (III) oxide (≈576eV) with binding energies of 577.21eV (20.22%) and 576.81eV (79.78%).

Ca2p

The samples shown in Figure 41 two distinct peaks with the higher binding energy confirming the presence of either Calcium Carbonates or phosphates (347.2 and 347.4eV respectively). All three samples show relatively similar levels of % atomic concentration on their surfaces with E2A showing the highest level 43.38% compared to E1A's 31.73% and D1A's 36.49%.

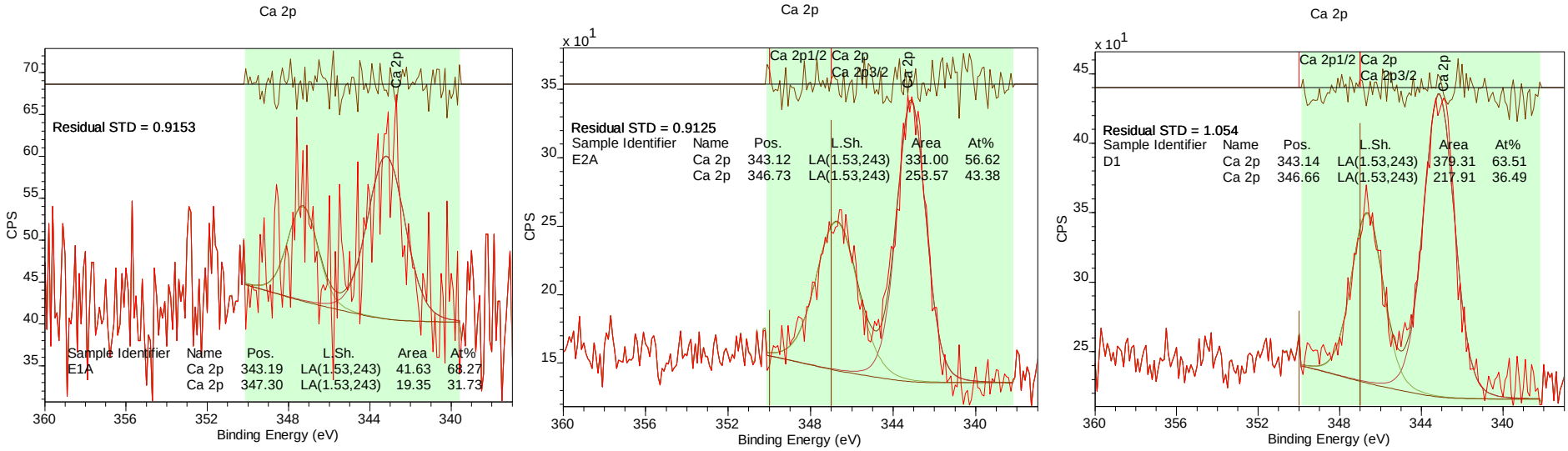

Figure 42: Ca2p spectra: E1A (left), E2A (middle) and D1A (right).

C1s

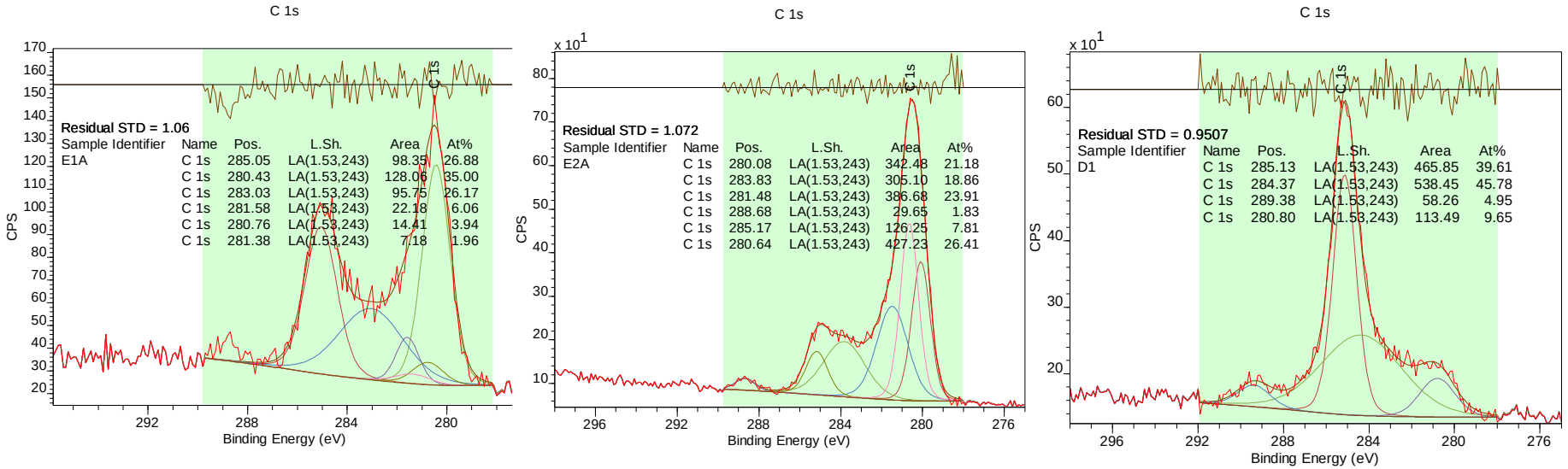

Figure 43: C1s spectra: E1A(left), E2(middle) and D1A(right).

Due to Carbon's presence in steel, and adventitious contamination from the sample's storage. There are a lot of C1s peaks within the three sample's spectra. All three samples have similar binding energy peaks with similar quantities with regards to the % atomic concentration.

4.3.TalySurf

Table 5 shows the results for both best case and worst-case samples (A and B), for the three samples, like the previous results 1-3 are measurements on samples A and 4-6 are on B. The anomalies/outliers are highlighted and subsequently excluded from the average calculations and standard deviation values (st dev) are rounded up to three decimal places.

Table 5: TalySurf results for the D1, E1 and E2 samples. The results highlighted in bold are the B samples.

		Ra	**Rq**	**Rp**	**Rv**	**Rt**	**Rmax**	**Rz**	**Rrms**	**Rsk**
E2 6491201	**1**	0.787	0.962	2.23	2.54	7.65	6.81	4.77	0.962	-0.476
	2	1.01	1.35	2.9	3.44	22.2	18.8	6.34	1.35	1.18
	3	0.802	0.996	2.47	2.55	6.9	6.43	5.02	0.996	-0.191
	4	0.912	1.1	2.48	2.73	8.73	8.73	5.21	1.1	-0.241
	5	0.871	1.07	2.09	2.86	6.41	5.78	4.95	1.07	-0.369
Average		0.877	1.096	2.434	2.824	10.378	9.31	5.258	1.096	-0.02
st dev		0.091	0.153	0.309	0.37	6.667	5.418	0.626	0.153	0.68
E1 6491201	**1**	0.856	1.05	2.35	2.56	6.47	5.98	4.91	1.05	-0.606
	2	0.701	0.88	2.33	2.33	6.19	6.11	4.66	0.88	-0.607
	3	0.754	0.963	1.95	2.59	5.98	5.84	4.54	0.963	-0.914
	4	**0.727**	**0.903**	**2.1**	**2.42**	**6.11**	**5.74**	**4.53**	**0.903**	**-0.426**
	5	**0.796**	**0.982**	**2.49**	**2.55**	**8.49**	**6.82**	**5.04**	**0.982**	**-0.262**
	6	**0.695**	**0.87**	**2.21**	**2.32**	**5.84**	**5.54**	**4.53**	**0.87**	**-0.415**
Average		0.755	0.942	2.239	2.462	6.514	6.005	4.702	0.942	-0.539
st dev		0.062	0.07	0.194	0.121	0.992	0.445	0.222	0.07	0.226
D1 B	**1**	**0.821**	**0.997**	**2.1**	**2.69**	**6.25**	**5.4**	**4.79**	**0.997**	**-0.129**
	2	**0.806**	**0.995**	**2.15**	**2.71**	**6.71**	**6.28**	**4.86**	**0.995**	**-0.327**
	3	**0.793**	**0.964**	**1.99**	**2.43**	**6.49**	**5.57**	**4.42**	**0.964**	**-0.105**
D1 A	**1**	0.76	0.934	2.31	2.44	7.74	5.94	4.74	0.934	-0.31
	2	0.892	1.18	2.89	3.45	14.1	14.1	6.34	1.18	0.182
	3	0.719	0.878	2.16	2.21	9.49	9.25	4.37	0.878	-0.0233
Average		0.799	0.992	2.267	2.655	8.464	7.757	4.92	0.992	-0.119
st dev		0.059	0.103	0.323	0.432	3.008	3.415	0.725	0.103	0.19

Table 6: Shows the average values for each sample best and worst-case samples.

	E2 6491202	E1 6491202	D1 2	D1	DP800	DP1000
Ra	0.876	0.755	0.807	0.790	0.909	0.832
Rq	1.096	0.941	0.985	0.997	1.122	1.002
Rp	2.434	2.238	2.08	2.453	2.245	2.11
Rv	2.824	2.461667	2.61	2.7	2.811667	2.675
Rt	10.378	6.513	6.483	10.443	7.085	6.775
Rmax						
Rz	9.31	6.005	5.75	9.763333	6.826667	5.905
Rrms	5.258	4.702	4.69	5.15	5.06	4.782
Rsk	1.096	0.941	0.985	0.997	1.122	1.001

Besides the single Ra value reading on E2 and D1A, there is very little deviation in terms of the readings. This is largely in part due to the release criteria and from these results it can be concluded that surface appearance has a small effect on the roughness of the surface, therefore this would not negatively impact coating performance. The negative Rsk indicates the presence of holes, this is because this value is a measure of symmetry (holes vs peaks) therefore a negative value indicates skew towards more holes therefore all three samples have holes on them. This can be compared with the initial values i.e., before the sample was sent through the CAPL line to identify whether the annealing atmospheres are responsible for these holes. Like the DP1000 sample, Rt>Rz therefore all samples analysed showed numerous single peaks/valleys, the same can be concluded for the Rv>Rp and the deeper valleys (data below the mean line).

4.4.DP800 Results Summary

XPS showed that for the Oxygen-based compounds (metal oxides and Carbonates) on the surfaces of the three samples (E1A, E2A and D1A), there was a similar atomic concentration between the edge samples from the 6491201 coils, but D1A showed the biggest atomic concentration. C1s compounds were also identified on the surface. Ca2p identified was entirely made up of Carbonates, which correlates to the data shown by the O1s spectra. Cr2p was also identified with D1A having the highest % atomic concentration. Despite the similar peak shapes E1A had a higher % atomic concentration that E2A however, D1A had the highest concentration of the three samples. Due to the concentration of iron (Fe) in AHSS samples, all samples showed high concentration, only D1A had a distinguishable amount i.e., the iron and the oxide's concentration. Si2p spectra confirmed the oxides shown in the O1s spectra as all three samples showed the presence of Si in its elemental form and an oxide compound with similar concentration. There were all metal nitrides of similar quantities on the surfaces of all three samples, due to the similar binding energies of Sn oxides, there were present on the surface, however the state of the oxides could not be established. TalySurf showed very small deviation between the samples collected from the two DP800 coils, this can attribute to the

release criteria from the production line, therefore it can be established that despite the difference in appearance, surface roughness values remain relatively unaffected.

4.5. Recommendations to improve future results

With regards to the improvements on the methods used for this dissertation, another area that needs to establish earlier would that sample preparation (grinding with a Silicon-based grinding paper), like the mount (Carbon).

Two quick characterisation methods for future samples include firstly, creating a reference library using accurate and reliable analysis methods such as XPS including a depth profile, this coupled with the reliability of this method allows confidence release of the material to the consumer given previous observations. This library would include the application evaluation of different samples i.e., best, and worst case to observe if there is a noticeable impact, this can determine if future samples are suitable for release. Other methods are FTIR ATR and Raman Spectroscopy, these have shorter setup times and are more accessible therefore have a better potential to be implemented into the processing line i.e., shorter analysis times. FTIR would involve collecting the oxide (by scratching) layer mixing it with ≈350mg KBr in a die, processed into a transparent disc and analysed to identify the chemical compositions and phases i.e., surface oxide phases.

Chapter Five

5. Discussion

The extent of the oxidation is dependent on the annealing atmosphere i.e., the availability of Oxygen within the processing line. This can be affected by the gas ratio which can be increased if the fan seals are compromised, this can be established by comparing gas volumes of the discoloured and non-discoloured samples. Previous work relating to surface appearance and performance coating i.e., the selective oxidation prior to hot dip galvanizing and the subsequent effect on reactive wetting and coating adherence concluded that Mn segregates to the surface, however this creates an inhibition layer whilst still exhibiting good coating performance (consistent target coating mass (g/m^2 per side). It is also worth noting that previous investigations used simulators and avoided exposing the samples to the atmosphere to minimise further oxidation therefore, the reproducibility with regards to the finished product's appearance cannot be certain.

Results from the optical microscope surface analysis and analysing the cross section using SEM at high magnification (µm) showed that despite the discolouration, the oxides' cross-sectional width were very small when observed using both the scanning electron and backscatter electron detector (BSE). Despite the BSE picking up on the inclusions that are formed through internal oxidation within the substrate, the surface oxide was relatively indistinguishable despite the difference in atomic density between the surface oxide and the substrate plus inclusions. Energy Dispersive X-ray Spectroscopy (EDS) was carried out on the cross section identifying some elements near the surface using spot scans, these elements were subsequently confirmed using XPS.

Given the Mn wt% (max 2.29 for DP1000 and 1.92 for DP800) coupled with the reactivity of Mn compared to the other alloying elements, the concentration of Mn oxides on the surface indicates the diffusing of Mn to the surface to form oxides. Mn oxides have very similar binding energies; MnO (641.4eV), Mn_2O_3 (641.4eV) and MnO_2 (641.8eV). Due to the due to the binding energy peaks being shifted for oxides, it is not possible to distinguish the oxidation state of Mn on the surface. For the Cr2p spectra, if Zn had been introduced to these samples as Cr overlap with Zn LMM Auger peaks, therefore, a Cr3p peak would be more suitable for peak fitting if the concentration is high enough. Presence of Ca in steels is for the refining of the Manganese sulphide (MnS) 'stringers', this is done to prevent the formation of MnS cracks which can be the site of fatigue cracks[16]. E1A showed three peaks indicating the presence of Sn metal and the oxides (SnO and SnO_2). The oxides have similar binging energies 486eV (SnO) and 486.6eV (SnO_2), therefore a valence spectrum is required to further distinguish between the two oxides. The spectrum, these spectra can be overlapped by Mo which is an alloying element in DP800 (0.02wt%). N1s peak shapes are known to be unusual, especially with surface oxynitrides, components are usually moved to higher binding energies. Any sample exposed to the atmosphere will have further oxidation on its surface, therefore a depth profile would have been a more preferrable option, another alternative would be to simulate the annealing process in a closed environment.

For O1s, three samples had higher peaks i.e., % atomic concentration at a similar binding energy ≈527eV, however C7025701's sample had the largest peak at ≈530eV indicating that this was the coil with the highest level of oxidation. DP1000 samples showed the smallest concentration for both oxides and Carbonates, with the maximum value of 30.20%. Ca2p had similar peaks across the four samples (DP1000, D1 (DP800), E1A and E2A) with the largest peak occurring at ≈343eV and one signifying the presence of Carbonates and/or phosphates on the surface (≈347eV). Cr2p had noisy spectrum shapes for all four samples, however DP1000 had the largest % atomic concentration (80%), with the DP800 samples having around 70%, however no distinction can be established with regards to the oxidation state i.e., whether the oxides are Cr (III) or Cr (IV). Mn2p showed two peak locations across all samples too with first peak occurring at ≈636eV and the second at ≈641ev indicating the presence of Manganese oxides. Due to the similarity between the binding energies of the Mn_xO_x oxides, a distinction cannot be established. However, DP800 showed a larger % atomic concentration with E2A (70.12%) and D1(65.45%), these values were from single readings therefore a repeat would be needed to evaluate their reliability and establish whether they were outliers or not. Given the wt% for Mn in DP1000 being higher than DP800, the larger %atomic concentration of other high affinity elements in DP 800 e.g., Cr would mean more oxides. DP1000 samples showed a dark appearance compared to the 'blue' appearance of DP800, this is consistent with the appearance of Mn oxides. Given the abundance of Fe and C in AHSS, the large concentration on the surface should come as no surprise, however the C1s values is affected by adventitious contamination from storing the samples in plastic containers therefore the quantity is not as reliable. Future work would consider a different method of

The major chemical composition differences for the DP800 and 1000 is that DP1000 contains more Mn whilst DP800 contains more Si. DP800 showed the most discolouration compared to the DP1000 samples, it is also worth noting the ULC samples appear to not have any issues with discolouration; they also happen to have the smallest wt% of Mn Si and Cr of the three. Given the reactivity of both Mn and Cr and the peak positions of the Mn and Cr spectra for all the DP1000 and DP800 spectra obtained through XPS, it can be concluded that these are the elements most responsible for diffusing to the surface. Due to the nature of the quantification method i.e., the peak fitting of the results the reliability of the results can be improved by carried out more analysis on different parts of the sample that based on discolouration (most of the surface discolouration is not uniform therefore a measurement can be compared between the extremely discoloured location compared to a 'clear' spot as observed under a microscope).

The reliability of the XPS would have been improved by repeating the readings for each of the location, due to time constraints concerning the availability of the equipment this could only be achieved for the B samples. Therefore, in terms of comparison, and an overall evaluation of reproducibility, both samples should have had a similar number of measurements carried out. Future work can make use of depth profiling, this allows the distinction of the external and internal oxidation to conclude whether the extent of oxidation is unique to the surface, if so, how much the quantity varies as you go deeper into the substrate. Binding energy occurred within the range of metal oxides for all the samples (529-530eV), metal oxides tend to have a narrower peak compared to those of Carbonates, therefore this allows a reliable distinction to be made. C1s the highest peak correlated with the binding energy typical of a C-C bond, this can be due to adventitious Carbon contamination. Sn3d XPS region has very similar binding energies (Sn metal (485.2eV), SnO (486eV), SnO_2 (486.6eV) which are distinguished using

the difference in their valence band spectra. F1s peak occurred within the binding energy range typical of metal fluorides (684-685.5eV), organic fluorine species are commonly observed surface contaminants, Ca2p binding energy peaks occur in the binding energy range typical of $CaCO_3$. Si2p spectra had a similar shape with one distinct peak occurring at >99eV, this indicated the presence of Si in its elemental form, Silicon is known for its detrimental effect on strip wettability during hot dipping [38]. Fe2p due to the compositional percentage of Fe in AHSS, it is expected that the CPS values be large, XPS can also allow the identification of the states in which the Fe is found. Mn2p due to the shape of the peaks given (there were no distinct peaks across all the samples analysed, a comparison can be made between the count values of the different chemical states. The values represented in the table are those of the oxide states, like those of Cr2p. Cr2p like the previous element, the values included for comparison are for the oxidation states Cr (III) and Cr (IV), so that a comparison can be made for the level of oxidation and the elements responsible and their relationship with surface appearance.

The biggest addition would be a depth profile taken for all the samples; due to the duration of this procedure a single profile can be obtained for the sample. This would enable a clearer picture of the contrast between external and internal oxidation to compare the extent and this can therefore be used when evaluating the impact of the processing line. For an improved accuracy with regards to the XPS spectra of Mn i.e., further distinguish between the oxides, Mn3s region would have to be collected too. It is also important to note that atmospheres with larger concentration of Oxygen result in more internal oxidation leaving fewer oxidised phases on the surface.

In conclusion results obtained through the analysis techniques shows that despite the appearance showing a massive departure from what a typical sample would appear like, the extent at a microscopic level is very minimal, the subsequent impact on surface roughness is shown to be minimal too as results obtained with the exceptions of distinct outliers show the values remain similar.

Chapter Six

6. Conclusion

- The surface discolouration is caused by the oxides formed when alloying elements diffuse to the surface and form ionic bonds with Oxygen.
- SEM showed that for all the samples (DP800 and 1000), the cross-sectional width of the oxide layer was very small, and the back scatter diffraction (BSE) did not provide a clear distinction between the substrate and the surface.
- EDS results identified the heavier elements (alloying elements) however majority of these were in the substrate.
- XPS results were compared between similar DP800 samples; E1, E2, and the C7025701 coil.
- XPS showed that despite the dissimilar appearance between samples of the same coil (6491201 edge samples E1 and E2) for the DP800 samples, the impact on the % atomic concentration was very minimal.
- However, the C7025701 coil with the dark grey appearance showed the greatest level of surface oxidation with high % atomic concentration for the high affinity alloying elements with both oxides and Carbonates on the surface.
- The DP800 grades showing the most discolouration were the edge samples compared to the mid-width.
- Surface roughness analysis (TalySurf) showed that there was minimal deviation in the Ra values for the samples selected as OK and NOK, this shows that discolouration has very little impact on the uniformity of the surface roughness values, Rsk values were predominantly negative across all six samples for the surface roughness, this signifies that there were a lot of holes across all samples. This was observed for both DP800 and DP1000 grades.
- Given that the oxide layer is minimal and will have minimal impact on performance, it is not economically viable to alter processing parameters such as annealing atmosphere.
- A cost-effective solution to this problem would be a sample reference library with previous values from the different analysis methods to be used as a guide to verify whether coils exhibiting this discolouration are suitable for the desired application.
- Another alternative would be the monitoring of the annealing atmosphere Oxygen potential to minimise discolouration, similar monitoring can be applied to the fan seals to ensure that the presence of Oxygen is minimised.

Future Work Recommendations

6.1. Improvements to current results.

To reduce the impact of further oxidation because of exposure to the atmosphere, samples can be investigated within a simulator and stored in anhydrous isopropyl alcohol to minimise the possibility of further surface oxidation. Initially the chemical composition of all the samples to be analysed must be known to relate this to the level of discolouration i.e., to see if there is a correlation. Annealing atmosphere and other exacting conditions must be continuously logged to establish if the seals are compromised during a run. This also allows the reliable establishment of the extent of the relationship between these wet atmospheres and discolouration. Finally, it is also worth noting that there are improvements that can be made with regards to gathering future data or reproducing these results. The C can be removed from the surface of the sample using Ar sputtering to improve the accuracy and reliability of the C1s spectra. The XPS results can be obtained from multiple locations to spot any outliers and confirm the reliability and reproducibility of the values obtained. Using EDS, sample spectrums can also be obtained to compare the chemical compositions of the external and internal oxidation so a comparison can be drawn between the oxides in a rich/poor environment (surface vs internal). Further work can be carried out to improve the reliability of the results and devising a technique for mounting that does not include an element within the AHSS samples i.e., the Carbon-based Bakelite would not be suitable for identifying the overall amount of Carbon within the samples. The more time elapsed when gathering data for EDS tends to lead to more reliable and accurate data, especially for the smaller weight percentages as this allows for more data values to be processed and therefore this leads to more defined peaks for the samples detected using the AutoID future. Lastly, the orientation of the samples must be maintained throughout, this can be achieved using a notch to ensure that analysis is carried out in the rolling direction for all samples. This allowed the investigation of the appearance in relation to the annealing atmosphere. Other methods of microscopy can also be used as an alternative, these include transmission electron microscopy (TEM), another form of spectroscopy to be used for analysis is glow discharge optical emission spectrometer (GDOES) to measure elemental composition profiles as a function of sputtering depth.

6.2. Depth profile

The following can be illustrated using XPS, this is a destructive analysis technique that allows the identification of the elements that have diffused to the surface and how this differs as you go further into the substrate. Surface oxides are formed in three stages: Oxygen chemisorption, formation of the oxide layer and lastly thickening of the oxide layer [19]. This allows the clear identification of the difference between the surface and internal oxidation; this is because whilst alloying elements such as **Mn** and **Cr** diffuse to the surface, the difference between the surface and substrate quantities could be negligible. Secondly, this form of analysis also allows the analysis of the inclusions that were observed when the sample's cross sections were analysed in SEM. Future work carried out with the XPS will have improved reliability and accuracy if more readings are carried out per sample. Given the time this would require it is recommended all samples be analysed in bulk and depth profiling carried out after, given the sensitivity of

this analysis method the time elapsed is justified by the quality of results and therefore these results can be retained as reference material for future samples of similar appearance.

6.3. Raman spectroscopy

If XPS is unavailable, an alternative would be to use Raman spectroscopy, whilst it is not as sensitive it still allows the identification of the oxides and their respective phases. Coupled by the quicker turnaround time and the economic viability of this form of analysis, Raman is a strong recommendation for future analysis for quality control purposes.

Raman allows the distinction to be made with regards to the phases the Mn and Cr oxides exist on the surface of these metals. These can in turn be used to predict their effects on different applications through consulting previous literature i.e., metal oxides and their influence on applications such as coating. It is also important that more samples from a similar batch are to be analysed as the slight variations in wavelength i.e., within the acceptable range signify a reliable data set. Spectra was retrieved from a variety of databases and cross referenced to determine the wavelength certain oxides exists in.

Raman spectroscopy is a non-destructive analysis technique at lower energies, it provides detailed information of the chemical structure by revealing the interactions based on the reaction of light with the chemical bonds within the AHSS. This method of spectroscopy is largely based on the nature in which light from a high intensity laser source scatters after interacting with an incident molecule [39].

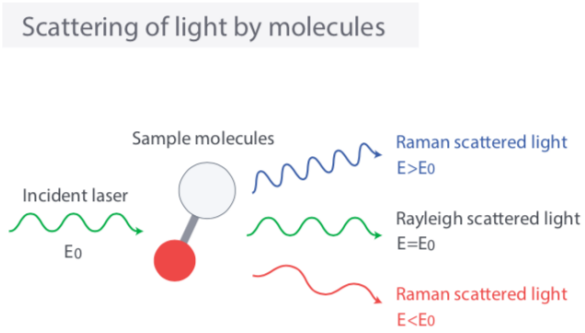

Figure 44: The interactions between light and bonds within the material undergoing analysis [40].

Rayleigh scattering occurs because most of the light will be the same wavelength as the laser source and therefore will not provide useful information. (0.0000001% is scattered at different wavelengths dependent on the chemical structure of the analyte [41]. The Raman spectrum shows the wavelength and intensity unique to molecular bond vibration, including individual and group bonds. A Raman spectrum can be sometimes referred to as a fingerprint for a molecule or material as it can be used to quickly and identify a material with distinction this can be confirmed by using the existing spectral library.

For the AHSS samples prepared the mapping from Raman should confirm the elements involved in the manufacturing of AHSS but it should also show the differences in the elements responsible for the discolouration as the surfaces have shown both dull and bright discolouration. Raman spectroscopy's other advantage is that it is both qualitative and

quantitative depending on the peak position and peak intensity. Where the intensity is directly linked with the concentration, this can be further refined by carrying out a calibration procedure to determine the relationship between intensity and concentration and subsequent routine measurements can be made to analyse the concentration.

6.4. Raman Results

The following preliminary results were observed using a laser with γ = 532nm, operating at a power of 0.013mW with exposure time of 2s to carry out a spot scan the size of the laser width. These initial parameters were chosen as they were optimal to protect the sample from destruction whilst also providing a suitable baseline within a reasonable frame of time. Subsequent analysis can employ a scanning technique as opposed to a spot scan to characterise greater surface area, distinguish the composition difference across the surface.

Manganese oxides (MnOx) typically occur in cryptocrystalline and fine-grained mixtures of different Mn-phases, Carbonates, silicates, and Fe oxides/hydroxides; this makes characterisation by standard methods challenging [42]. Raman spectroscopy allows the identification of the different phases the ionic bonds exist in on the surface of the AHSS samples. In the Raman spectra of MnOx, three main regions can be distinguished: (a) 200-450 cm^{-1} range (skeletal vibrations); (b) the 450-550 cm^{-1} range (deformation modes of the Mn-O-Mn chains in the octahedral lattice); (c) the 550-750 cm^{-1} range (stretching modes of the Mn-O bonds in the MnO_6 octahedra [43].

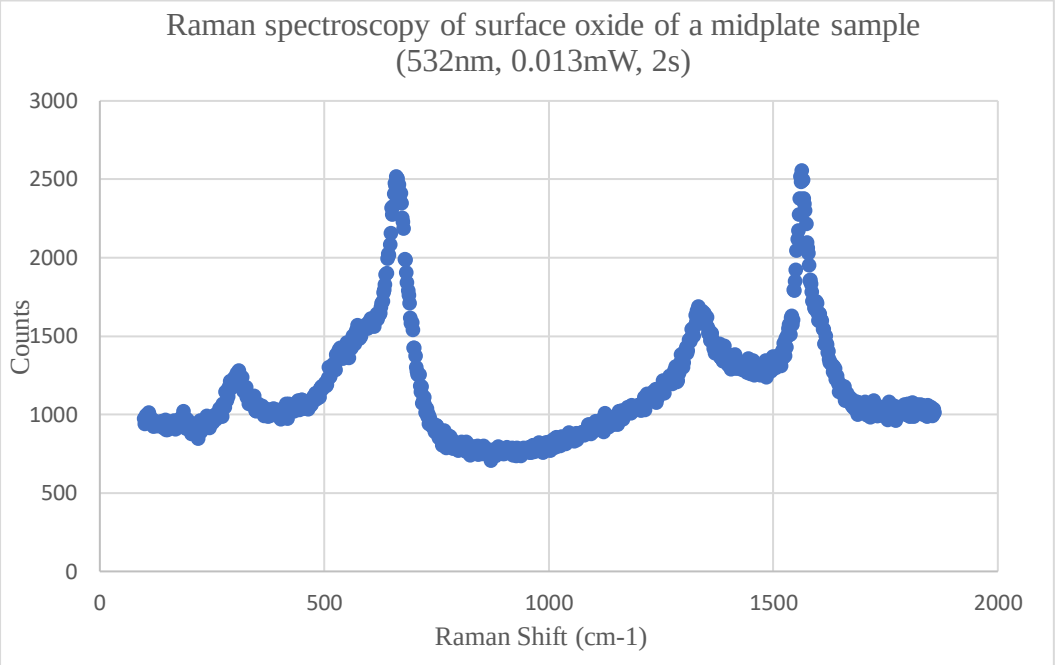

Figure 45: Raman spectroscopy of the surface oxide of the midplate sample.

The midplate sample had distinct peaks at 308.0, 660.8, 1339.3 and 1566.4 cm^{-1} were identified and singled out (due to their high count/intensity). These were measured with a tolerance of (±5 cm^{-1} and identified using pre-existing wavelength numbers from public libraries curated from previous work using Raman that has achieved similar results.

Surface oxides in Advanced High Strength Steels (AHSS): Effects on applications and appearance.

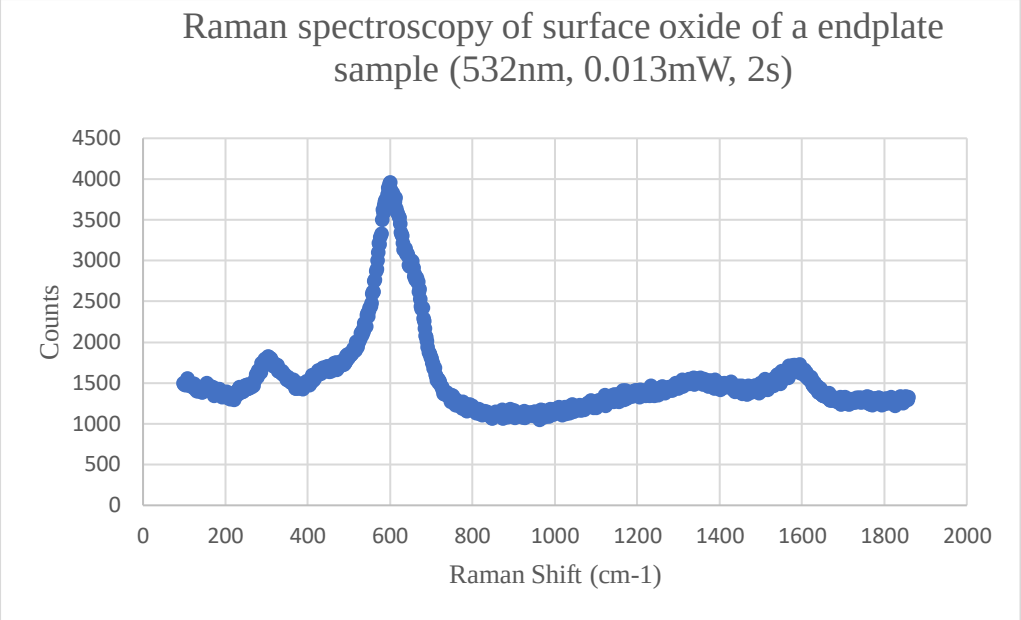

Figure 46:Raman spectroscopy of the surface oxide of the endplate sample.

The midplate sample had four distinct peaks of 305.1, 600.8 and 1587.1 cm^{-1}; the same tolerance value was used for both samples (±5 cm^{-1}) were used. It is important to note that whilst the first two peaks have a higher count for the midplate, the subsequent peaks for both samples have similar figures in terms of the Raman Shift,

It is worth noting that broadening of the peaks for both samples can be attributed to the photo-induced or thermal-induced chemical reactions.

6.5.FTIR ATR

This method of analysis would be preferrable since it has a relatively shorter analysis time compared to XPS and is more accessible to carry out. This method of analysis is therefore more adaptable for a processing line given the portability of the analysis machine (a computer equipped with processing software and the machine). There are four sampling techniques in FTIR, namely, transmission, attenuated total reflection (ATR), specular reflection and diffuse reflectance. ATR allows analysis of the composition of the surface, in this case the oxide layer. The impact of the results obtained through this method of analysis are similar in terms of quantification of the elemental composition within the oxide layer by XPS, however are not as sensitive.

FTIR is a non-destructive method of analysis that involves the use of infrared spectroscopy analysis of IR radiation that has both been absorbed by the sample and that which has passed through the sample, the resulting signal developing a spectrum (absorption peaks) representing a molecular ‘fingerprint’ of the sample [44]. This method of spectroscopy allows accurate analysis of structures as each structure produces its own specific fingerprint. FTIR allows the identification (qualitative analysis) of unknown materials (because of the unique combination of atoms, no two compounds can produce the same IR spectrum), quality and consistency of the samples and the number of components in a mixture (which is detected by the size of the peaks) [45]. The standard method to prepare solid samples for FTIR is using KBr (potassium

bromide) [46]. The next step is to carry out a background scan to obtain a background spectrum, by collecting an interferogram and its subsequent conversion to frequency data by inverse Fourier transformation [46]. The background spectrum allows the differentiation of the elements within the solvent as compared to those within the samples being analysed and any contaminations if present. The next step is to collect a single beam spectrum of the sample, noting this spectrum will contain the background spectrum and these absorption bands will need to be subtracted to isolate those of the sample.

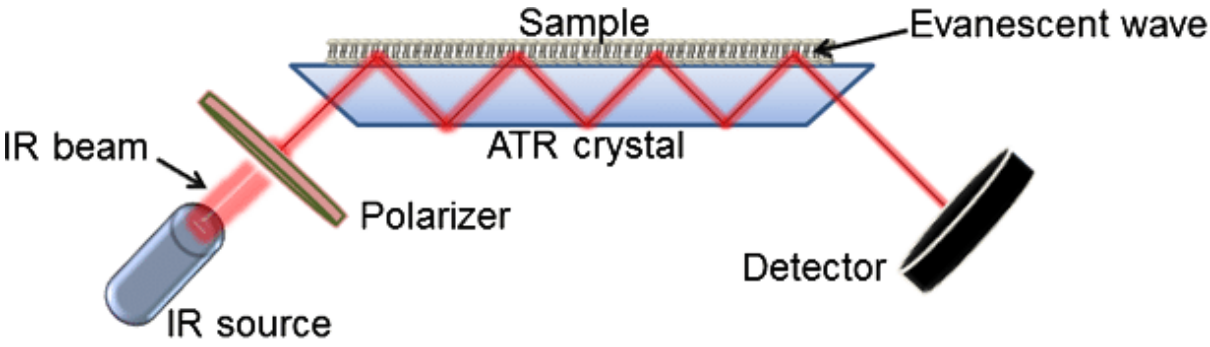

Figure 47: Typical setup for FTIR ATR analysis

This is useful to the research carried out, combined with the other methods of analysis composition within the oxides can be confidently identified. In relation to this research FTIR, will be of use when it comes to determining the elements within the oxides and the quantity and this can further explain the difference in shades on the surface of the samples. FITR is already employed in different sectors as a quality control/assurance measure; therefore, results will not only be accurate but they will also be reproducible, therefore the samples collected from the different sections of the plates there should be consistency within the fingerprint, however, the amount can be expected to fluctuate [47].

This method of analysis required analysis of the cleaned sample using the Perkin Elmer 2 FTIR ATR machine, initially the crystal was cleaned to ensure there would be no contaminants detected that were not part of the sample. The samples were named accordingly i.e., 'midplate', 'endplate' etc. Scan parameters were initially set to run at 4000cm^{-1} to 450 cm^{-1} using 4 scans. These were the parameters used for the initial evaluation run with any changes to be made for the future analysis if this analysis method was deemed suitable for further sample analysis. Initially a background scan is running to ensure that the background spectra of diamond ATR in air was acquired before proceeding with analysis. Depending on the number of scans chosen, the progress after each scan will be shown as a % below the acquired spectra.

For the sample analysis, select a suitable shoe for the sample and attach onto the swing arm, then using the force bar as reference, tighten the swing arm until the green bar is if possible. This signifies the tightness of the sample against the crystal, which is important when trying to acquire reliable results. Finally, pressing the scan button provides a preview of the spectra and the second press of the button allows the user to record the spectra acquired. Before swapping samples and repeating the above procedure to analyse subsequent samples it is important that the crystal is cleaned with distilled water as this would remove any debris/contaminants on the

crystal. Avoid using harsh chemicals such as ethanol as these will have a detrimental effect on the oxide layer and therefore negatively impact any further analysis. If your results show a lot of noise or vary massively from those in previous literature it is important that a ready check be performed to ensure the instrument is operating as desired concerning the wavenumber precision, check on noise, throughput, and contamination. Data interpretation was carried out using Spectrum software.

6.6.FTIR Results

FTIR showed broad and overlapping bands and this made unique identification of the mineral difficult considering there was likely to be a mixture of oxides on the surface. Due to the setup of the machine, it was also impossible to pinpoint the area under analysis and therefore a relationship between colour and the oxides present could not be confidently established. Future sample preparation to improve the accuracy of the spectra would include collecting samples off the surface, grinding it down and mixing it with no more than 20mg of mineral oil (nujol) for analysis by transmission. An alternative is Potassium bromide (KBr) which is the most widely used material for sample preparation, this involves using between 1-3mg of ground material mixed thoroughly with ≈350mg of ground KBr, transferred to a die, pressed at 12,000psi for 1-2 minutes (can also be evacuated). The KBr is then recrystallised into a clear glass disk which can then be analysed by transmission. Throughout the analysis it is important that the samples are always in direct contact with the ATR crystal, to ensure the evanescent wave/bubble is always in contact with the sample.

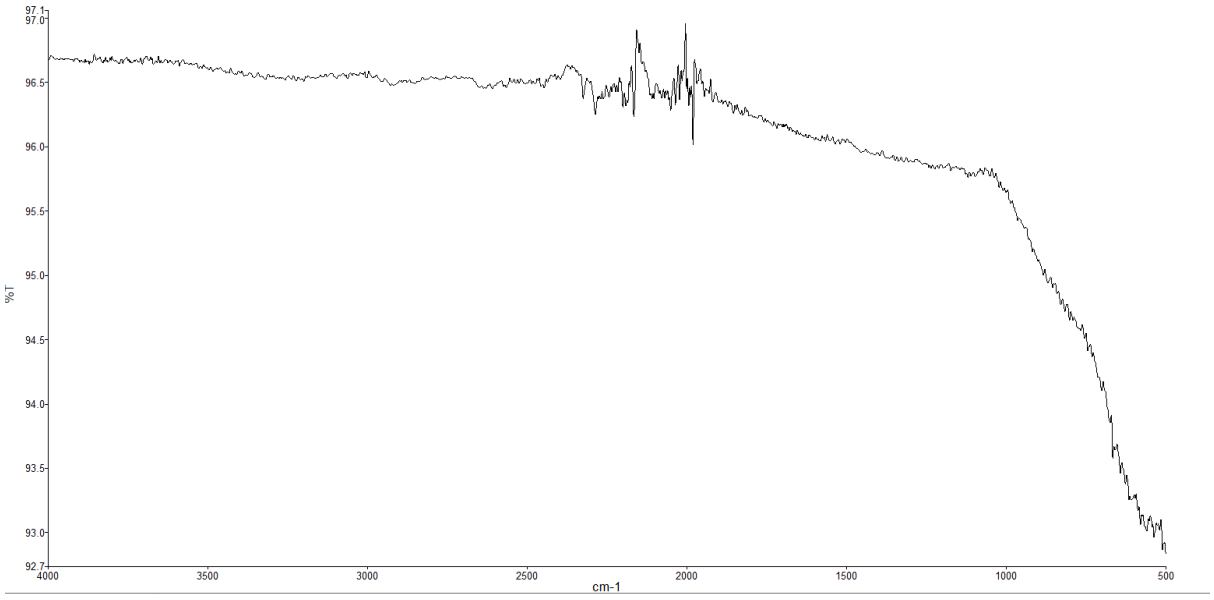

Figure 48: FITR spectrum of the end plate sample.

References

[1] S. Keeler, M. Kimchi, and P. J. Mooney, “Advanced High-Strength Steels Apllication Guidelines Version 6.0,” *World Auto Steel*, vol. 6, no. September, p. 314, 2017.

[2] S. Swaminathan and M. Spiegel, “Thermodynamic and kinetic aspects on the selective surface oxidation of binary, ternary and quarternary model alloys,” *Applied Surface Science*, vol. 253, no. 10, pp. 4607–4619, 2007, doi: https://doi.org/10.1016/j.apsusc.2006.10.031.

[3] A. Broddefalk, K. Jenkins, N. Silk, and M. Lindenmo, “The influence of dew point during annealing on the power loss of electrical steel sheets,” *Journal of Magnetism and Magnetic Materials*, vol. 320, pp. 665–668, 2008, doi: 10.1016/j.jmmm.2008.04.027.

[4] E. van der Aa and W. Stijger, “Contact resistance of DP800CR CAPL material with varying surface appearance,” vol. 31, no. 0, pp. 1–6, 2019.

[5] “High strength steels offer the potential to lower CO2 emissions in the automotive industry | Materials Science and Engineering | The University of Sheffield.” https://www.sheffield.ac.uk/materials/news/high-strength-steels-offer-potential-lower-co2-emissions-automotive-industry (accessed Jun. 04, 2021).

[6] R. Khondker, A. Mertens, and J. R. Mcdermid, “Effect of annealing atmosphere on the galvanizing behavior of a dual-phase steel,” *Materials Science and Engineering A*, vol. 463, pp. 157–165, 2007, doi: 10.1016/j.msea.2006.09.116.

[7] “Alloying Elements in Steel | INFORMATION ON ENGINEERING STEEL.” https://ambhe.com/alloyingelements/ (accessed Jun. 04, 2021).

[8] “Most Common Alloying Elements in Steel | Diehl Tool Steel, Inc.” https://www.diehlsteel.com/technical-information/effects-of-common-alloying-elements-in-steel/ (accessed Jun. 04, 2021).

[9] G. Badinier, C. W. Sinclair, S. Allain, F. Danoix, and M. Gouné, “The Mechanisms of Transformation and Mechanical Behavior of Ferrous Martensite,” in *Reference Module in Materials Science and Materials Engineering*, 2017. doi: 10.1016/b978-0-12-803581-8.02518-2.

[10] R. Sagl, A. Jarosik, G. Angeli, T. Haunschmied, G. Hesser, and D. Stifter, “Tailoring of oxide morphology and crystallinity on advanced high-strength steel surfaces prior hot-dip galvanizing,” *Acta Materialia*, vol. 72, pp. 192–199, 2014, doi: https://doi.org/10.1016/j.actamat.2014.03.037.

[11] X. Vanden Eynde, J. P. Servais, and M. Lamberigts, “Investigation into the surface selective oxidation of dual-phase steels by XPS, SAM and SIMS,” *Surface and Interface Analysis*, vol. 35, no. 12, pp. 1004–1014, Dec. 2003, doi: 10.1002/sia.1639.

Surface oxides in Advanced High Strength Steels (AHSS): Effects on applications and appearance.

[12] J.-H. Schmitt and T. Iung, “New developments of advanced high-strength steels for automotive applications,” *Comptes Rendus Physique*, vol. 19, no. 8, pp. 641–656, Dec. 2018, doi: 10.1016/J.CRHY.2018.11.004.

[13] “Tata Steel - Metallic coated - Advanced high-strength steel.” https://www.tatasteeleurope.com/en/products/automotive/metallic-coated/ahss-uhss (accessed Oct. 19, 2019).

[14] A. Abraham, “Metallic Material Trends in the North American Light Vehicle,” *Autosteel*, 2015.

[15] H. K. D. H. Bhadeshia and M. Peet, “Oxide on Steel and Tempering Colours.” https://www.phase-trans.msm.cam.ac.uk/2008/Oxide/Oxide.html (accessed Oct. 18, 2019).

[16] “Manganese Sulphide Inclusions in Steel: Part One :: Total Materia Article.” https://www.totalmateria.com/page.aspx?ID=CheckArticle&site=kts&NM=443 (accessed Mar. 05, 2020).

[17] S. State, “Chapter 7 Wear,” pp. 429–509, 1981, doi: 10.1016/s0167-8922(08)70680-1.

[18] R. Wilson, “Part 1 Friction of Metals,” *influence of oxide films on metallic friction*, vol. 212, no. 1111, p. 450, 1950.

[19] F. Yusof and M. F. Jamaluddin, “Welding Defects and Implications on Welded Assemblies,” *Comprehensive Materials Processing*, pp. 125–134, Jan. 2014, doi: 10.1016/B978-0-08-096532-1.00605-1.

[20] M. Maderthaner, A. Jarosik, G. Angeli, and R. Haubner, “Effect of dew point on the selective oxidation of advanced high strength steels,” *Materials Science Forum*, vol. 891 MSF, no. March, pp. 292–297, 2017, doi: 10.4028/www.scientific.net/MSF.891.292.

[21] G. Seyed Mousavi and J. R. McDermid, “Selective Oxidation of a C-2Mn-1.3Si (Wt Pct) Advanced High-Strength Steel During Continuous Galvanizing Heat Treatments,” *Metallurgical and Materials Transactions A: Physical Metallurgy and Materials Science*, vol. 49, no. 11, pp. 5546–5560, Nov. 2018, doi: 10.1007/s11661-018-4854-2.

[22] G. Seyed Mousavi and J. R. McDermid, “Selective Oxidation of a C-2Mn-1.3Si (Wt Pct) Advanced High-Strength Steel During Continuous Galvanizing Heat Treatments,” *Metallurgical and Materials Transactions A: Physical Metallurgy and Materials Science*, vol. 49, no. 11, pp. 5546–5560, 2018, doi: 10.1007/s11661-018-4854-2.

[23] “Thermo Scientific XPS: What is XPS.” https://xpssimplified.com/whatisxps.php (accessed Jan. 30, 2020).

[24] M. I. De Barros *et al.*, “Friction reduction by metal sulfides in boundary lubrication studied by XPS and XANES analyses,” *Wear*, vol. 254, no. 9, pp. 863–870, 2003, doi: 10.1016/S0043-1648(03)00237-0.

[25] H. Konno, *Chapter 8 - X-ray Photoelectron Spectroscopy*. Tsinghua University Press Limited, 2016. doi: 10.1016/B978-0-12-805256-3.00008-8.

Surface oxides in Advanced High Strength Steels (AHSS): Effects on applications and appearance.

[26] Y. Okamoto, Y. Nitta, T. Imanaka, and S. Teranishi, “Surface characterisation of nickel boride and nickel phosphide catalysts by X-ray photoelectron spectroscopy,” *Journal of the Chemical Society, Faraday Transactions 1: Physical Chemistry in Condensed Phases*, vol. 75, no. 0, pp. 2027–2039, Jan. 1979, doi: 10.1039/F19797502027.

[27] “Basic Quantification of XPS Spectra,” 2008.

[28] “Scanning Electron Microscopy - Nanoscience Instruments.” https://www.nanoscience.com/techniques/scanning-electron-microscopy/ (accessed Jan. 31, 2020).

[29] “Scanning Electron Microscope - Advantages and Disadvantages in Imaging.” https://www.microscopemaster.com/scanning-electron-microscope.html (accessed Jan. 16, 2020).

[30] “ZEISS SEM, FIB-SEM and Ion Beam Microscopy.” https://www.zeiss.com/microscopy/int/products/scanning-electron-microscopes.html (accessed Jan. 16, 2020).

[31] J. Bergström, *Experimental Characterization Techniques*. 2015. doi: 10.1016/b978-0-323-31150-2.00002-9.

[32] “Surface Roughness Chart: Understanding Surface Finish in Manufacturing.” https://www.rapiddirect.com/blog/surface-roughness-chart/ (accessed Mar. 01, 2021).

[33] J. Konopka, “Quantitative Differentiation of Three Iron Oxides by EDS,” *Microscopy and Microanalysis*, vol. 19, no. S2, pp. 1046–1047, 2013, doi: 10.1017/s1431927613007228.

[34] “AXIS Supra+ X-ray photoelectron spectrometer.” https://www.kratos.com/products/axis-supra-xps-surface-analysis-instrument (accessed Apr. 01, 2021).

[35] C. Wright *et al.*, “Tin Oxides: Insights into Chemical States from a Nanoparticle Study,” 2017, doi: 10.1021/acs.jpcc.7b05013.

[36] “XPS Interpretation of Nitrogen.” https://xpssimplified.com/elements/nitrogen.php (accessed Apr. 01, 2021).

[37] “XPS Interpretation of Iron.” https://xpssimplified.com/elements/iron.php (accessed Apr. 01, 2021).

[38] J. Mahieu, B. C. De Cooman, and S. Claessens, “Galvanizability of high-strength steels for automotive applications,” *Metallurgical and Materials Transactions A: Physical Metallurgy and Materials Science*, vol. 32, no. 11, pp. 2905–2908, 2001, doi: 10.1007/s11661-001-1042-5.

[39] E. J. Schindelholz, H. Cong, C. F. Jove-Colon, S. Li, J. A. Ohlhausen, and H. K. Moffat, “Electrochemical aspects of copper atmospheric corrosion in the presence of sodium chloride,” *Electrochimica Acta*, vol. 276, pp. 194–206, Jun. 2018, doi: 10.1016/J.ELECTACTA.2018.04.184.

Surface oxides in Advanced High Strength Steels (AHSS): Effects on applications and appearance.

[40] "Lesson 1. Basic of Raman scattering | Nanophoton corp." https://www.nanophoton.net/raman-spectroscopy/lessons/lesson-1 (accessed Jan. 31, 2020).

[41] "What is Raman Spectroscopy?" https://www.horiba.com/en_en/raman-imaging-and-spectroscopy/ (accessed Jan. 15, 2020).

[42] S. Bernardini, F. Bellatreccia, A. Casanova Municchia, G. Della Ventura, and A. Sodo, "Raman spectra of natural manganese oxides," *Journal of Raman Spectroscopy*, vol. 50, no. 6, pp. 873–888, Jun. 2019, doi: 10.1002/jrs.5583.

[43] C. M. Julien, M. Massot, and C. Poinsignon, "Lattice vibrations of manganese oxides. Part I. Periodic structures.," *Spectrochim Acta A Mol Biomol Spectrosc*, vol. 60, no. 3, pp. 689–700, Feb. 2004, doi: 10.1016/s1386-1425(03)00279-8.

[44] "FTIR Spectroscopy Basics | Thermo Fisher Scientific - UK." https://www.thermofisher.com/uk/en/home/industrial/spectroscopy-elemental-isotope-analysis/spectroscopy-elemental-isotope-analysis-learning-center/molecular-spectroscopy-information/ftir-information/ftir-basics.html (accessed Jan. 24, 2020).

[45] "How an FTIR Spectrometer Operates - Chemistry LibreTexts." https://chem.libretexts.org/Bookshelves/Physical_and_Theoretical_Chemistry_Textbook_Maps/Supplemental_Modules_(Physical_and_Theoretical_Chemistry)/Spectroscopy/Vibrational_Spectroscopy/Infrared_Spectroscopy/How_an_FTIR_Spectrometer_Operates (accessed Jan. 24, 2020).

[46] N. Birkner, "How an FTIR Spectrometer Operates," *UC Davis ChemWiki*, pp. 1–11, 2011.

[47] "FT-IR Spectroscopy." https://www.newport.com/n/introduction-to-ftir-spectroscopy (accessed Jan. 31, 2020).